Design, Build and Test of an Axial Flow Hydrokinetic Turbine with Fatigue Analysis

by
Jerod Ketcham

B.S., Mechanical Engineering
Wichita State University, 1997

Submitted to the Department of Mechanical Engineering and the Department of Materials Science and Engineering in Partial Fulfillment of the Requirements for the Degrees of

Naval Engineer

and

Master of Science in Materials Science and Engineering

at the Massachusetts Institute of Technology
June 2010

Signature of Author_____
Department of Mechanical Engineering
May 7, 2010

Certified by_____
Mark Welsh
Professor of Naval Architecture
Thesis Supervisor

Certified by_____
Richard W. Kimball
Thesis Supervisor

Certified by_____
Ronald G. Ballinger
Professor of Materials Science and Engineering and Nuclear Science and Engineering
Thesis Supervisor

Accepted by_____
David E. Hardt
Chairman, Departmental Committee on Graduate Students
Department of Mechanical Engineering

Accepted by_____

Chairman, Departmental Committee on Graduate Students
Department of Materials Science and Engineering

DESIGN, BUILD AND TEST OF AN AXIAL FLOW HYDROKINETIC TURBINE WITH FATIGUE ANALYSIS

by

JEROD KETCHAM

Submitted to the Department of Mechanical Engineering and the Department of Materials Science and Engineering on May 7, 2010 in partial fulfillment of the requirements for the degrees of Naval Engineer and Master of Science in Materials Science and Engineering

ABSTRACT

OpenProp is an open source propeller and turbine design and analysis code that has been in development since 2007 by MIT graduate students under the supervision of Professor Richard Kimball. In order to test the performance predictions of OpenProp for axial flow hydrokinetic turbines, a test fixture was designed and constructed, and a model scale turbine was tested. Tests were conducted in the MIT water tunnel for tip speed ratios ranging from 1.55 to 7.73. Additional code was also written and added to OpenProp in order to implement ABS steel vessels rules for propellers and calculate blade stress. The blade stress code was used to conduct a fatigue analysis for a model scale propeller using a quasi-steady approach.

Turbine test results showed that OpenProp provides good performance predictions for the on-design operational condition but that further work is needed to improve performance predictions for the off-design operational condition. Fatigue analysis results show that reasonable estimates of propeller blade fatigue life can be obtained using a relatively simple method. Calculated blade stress distributions agree with previously published data obtained with more sophisticated and time consuming calculation techniques.

Thesis Supervisor: Mark Welsh
Title: Professor of Naval Architecture

Thesis Supervisor: Richard W. Kimball

Thesis Supervisor: Ronald G. Ballinger
Title: Professor of Materials Science and Engineering and Nuclear Science and Engineering

TABLE OF CONTENTS

TABLE OF CONTENTS 3
TABLE OF FIGURES 4
TABLE OF TABLES 5
Introduction 6
Chapter 1 –Development, Capability and Limitations of OpenProp 7
Development of OpenProp 7
Capability of OpenProp 7
Limitations of OpenProp 8
Chapter 2 – Hydrokinetic Turbine Design and Construction 9
Chapter 3 – Test Procedure, Results and Comparison 11
Test Procedure 11
Results and Comparison 17
Chapter 4 – Implementation of ABS Steel Vessel Rules for Blade Thickness 18
Rule Implementation in OpenProp 19
Limitations 19
Moment of Inertia Calculation 19
Chapter 5 – Calculation of Blade Stress 21
Theory 21
Implementation 24
Results 26
Chapter 6 – Fatigue Analysis 30
Cyclic Load 30
Fatigue Failure 35
Chapter 7 – Test Fixture Design and Construction 38
MECHANICAL 38
Thrust/Torque Sensor 38
Output Shaft Configuration 41
Drive Shaft Configuration 42
Housings 43
ELECTRICAL 44
Slip Rings 44
Amplifiers 45
Motor 45
Controller 48
CONSTRUCTION 50
References 52
Appendix A – Codes 53
Moment of Inertia Calculation 53
Centrifugal Force Calculation 56
Stress Calculation 57
Blade Stress Plots 59
Usage Script 61
Appendix B – Equipment Data Sheets 62
Appendix C – Drawings 62

TABLE OF FIGURES

Figure 1: Thrust Calibration 11
Figure 2: Torque Calibration 12
Figure 3: Spectrum Analysis–600RPM, 1.69m/s 12
Figure 4: Friction Torque 13
Figure 5: Measured Torque – No Correction 14
Figure 6: Test Section Flow Speed Determination 16
Figure 7: Results 17
Figure 8: Blade Section with Lift and Flow Velocity Vectors 21
Figure 9: Blade Section Showing Lift Resolved into Axial and Tangential Components 22
Figure 10: Bending Moments Components 23
Figure 11: Total Bending Moments about Centroidal Axes 24
Figure 12: Distorted Root Section 25
Figure 13: Undistorted Root Section 25
Figure 14: Calculation of Elemental Area Properties 26
Figure 15: On Design Root Section Stress 27
Figure 16: On Design Suction Side Stress: $J_s=0.75$, $V_S=1.5m/s$, $n=8rev/s$, $D=0.25m$ 27
Figure 17: On Design Pressure Side Stress: $J_s=0.75$, $V_S=1.5m/s$, $n=8rev/s$, $D=0.25m$ 28
Figure 18: Off Design Suction Side Stress: $J_s=0.40$, $V_S=1.5m/s$, $n=15rev/s$, $D=0.25m$ 28
Figure 19: Off Design Pressure Side Stress: $J_s=0.40$, $V_S=1.5m/s$, $n=15rev/s$, $D=0.25m$ 29
Figure 20: Sectored, Single Screw Ship Wake 31
Figure 21: Original Inflow Velocities 31
Figure 22: New Inflow Velocities 31
Figure 23: Pressure Side Blade Stress for Each Wake Sector 32
Figure 24: Point of Maximum Tensile Stress 33
Figure 25: Maximum Blade Stress versus Angular Position for Various Ship Speeds ..... **Error! Bookmark not defined.**
Figure 26: S-N Curve for NiAl Bronze 35
Figure 27: Operational Profile for DDG51 35
Figure 28: Example Operational Profile Used for Calculations 36
Figure 29: Time at Various Stress Levels 36
Figure 30: Provided Sensor 39
Figure 31: Stress from Axial Load on Sensor (50lbf applied) 40
Figure 32: Stress from Torque Load on Sensor (12ft-lbf applied) 41
Figure 33: Output Shaft Configuration 42
Figure 34: Driveshaft and Bearing Assembly with Brush Blocks and Slip Rings 43
Figure 35: Installed Slip Rings and Brushes 44
Figure 36: K089300-7Y Torque Speed Curve 46
Figure 37: Output Power Capability 47
Figure 38: Limiting Current 48
Figure 39: Electrical Components 49
Figure 40: Schematic of Enclosure Electrical Components 50
Figure 41: Completed Test Fixture in Operation 51

TABLE OF TABLES

Table 1: Development History of OpenProp 7
Table 2: Key Turbine Parameters 10
Table 3: Test Tip Speed Ratios 14
Table 4: Test Fixture Limitations 38

Introduction

Since 2007, graduate students at the Massachusetts Institute of Technology (MIT) have been developing an open source propeller and turbine design and analysis tool under the supervision of Professor Richard Kimball. The tool is a set of open source MATLAB® scripts published under the GNU General Public License which are capable of performing design and analysis studies for open and ducted propellers as well as axial flow turbines. This suite of MATLAB® scripts is called OpenProp. OpenProp propeller design capabilities include performing parametric studies of propellers using various propeller diameters, number of blades and rotation speeds. Propeller analysis features include performing off-design and cavitation analyses. A gap in OpenProp capabilities was the inability to evaluate the structural adequacy of a propeller or turbine. This project added two new modules. One module implements American Bureau of Shipping (ABS) steel vessel rules for propellers and the other calculates the blade surface stress.

Validation of OpenProp turbine and propeller performance predictions is limited. The portion of the code suite which designs ducted propellers has been validated against the US Navy's PLL code with excellent correlation. Several experiments have been done to validate open propeller performance predictions using a modified trolling motor apparatus. One test had been performed, with limited success, of an axial flow turbine. No tests had been performed for ducted propellers. Because of this lack of experimental validation of OpenProp, it became necessary to design and construct a propeller and turbine test fixture that is robust and can easily be used to test open and ducted propellers as well as turbines. This project provided a test fixture, funded by MIT SeaGrant, which can be used in a water tunnel or tow tank to provide experimental performance results which can be used to validate OpenProp performance predictions.

OpenProp implements the vortex lifting line method to quickly achieve a propeller or axial flow turbine design. The lifting line method of propeller design has some limitations but is an excellent method to obtain an initial design which can be refined using more sophisticated design techniques. In the spirit of providing initial design estimates, this project also completed a quasi-steady fatigue analysis and predicted the fatigue life of a propeller.

This paper presents the results of testing, blade stress calculations and fatigue analysis.

Chapter 1 –Development, Capability and Limitations of OpenProp

Development of OpenProp

OpenProp had its genesis in a code called MPVL which was a code which added graphical user interfaces to PVL which was developed by Kerwin for his propellers course at the Massachusetts Institute of Technology (MIT), Reference 3. Since that time significant capability has been added to the code and additional features and capability are being developed.

OpenProp uses a lifting line method to model blade circulation, Reference 11. The lifting line technique has been well established and was implemented by Kerwin for preliminary parametric propeller design for the US Navy in a code called PLL. OpenProp development sought to expand and enhance the capabilities of Kerwin's code and make the software more user friendly. A full explanation for the theory of operation of OpenProp has been given by Epps et.al., Reference 7.

Capability of OpenProp

A table showing the development history and current capability of OpenProp is shown below.

Date	Event	Persons Responsible	Description
2001	PVL Developed	J.E. Kerwin	Lifting line design code used for Kerwin's propeller class at MIT
2007	MPVL Developed (Later renamed OpenProp v1.0)	H. Chung K.P. D'Epagnier	MATLAB version of PVL which incorporated GUIs for parametric and blade row design and geometry routines for CAD (Rhino) interface. This code used a Lerb's criteria optimizer. Reference 3 and Reference 5.
2008	Cavitation Analysis Routines Developed	C.J. Peterson	Using Mark Drela's XFOIL, routines and executables were developed for conducting propeller cavitation analysis. Reference 15.
2008	OpenProp v2.0	J.M. Stubblefield	Added capability for ducted propeller design. Reference 17.
2009	OpenProp v3.0	B.P. Epps	Incorporated routines of Peterson, added off-design analysis, corrected errors and added ability to design axial flow turbines with or without blade chord optimization. Theory described in Reference 6.
2010	Contra-Rotating Propeller Design	D. Laskos	Added the capability for contra-rotating propeller design with cavitation analysis. Reference 14.

Table 1: Development History of OpenProp

This project added the capability to calculate blade stress and implement ABS rules for propellers. Epps continues to refine and expand OpenProp capabilities and is currently working on codes to predict propeller performance during shaft reversals.

Limitations of OpenProp

OpenProp uses the lifting line method to model the blade circulation. There are limits in regard to using this method in propeller design.

1. Constant Radius Vortex Helix – In the implementation of the lifting line method, the trailing vorticity is assumed to be of constant radius. For propellers, it is known that the trailing vorticity helix radius actually decreases. This simplification has been made to ease the complexity of calculating the influence of the trailing vorticity on the blade itself and the other blades that make up the propeller. The errors introduced with this simplification are relatively minor as shown in the experimental data comparison in this paper and by Stubblefield 2008 in his comparison of OpenProp predictions to a more established propeller design code.
2. Blade Geometry – OpenProp uses only one foil series to generate blade sections that produce the required lift. The series used is a modified NACA 65A010, modified to increase the blade thickness at the trailing edge. Section camber and chord are adjusted to produce the desired circulation distribution. Other foil series could be used provided that data for them is available and entered into OpenProp.

Chapter 2 – Hydrokinetic Turbine Design and Construction

In propeller design the overall objective is to maximize the thrust produced while minimizing the torque required to produce it. In turbine design the goal is to maximize the torque and minimize the thrust. A procedure which can be used with OpenProp for turbine design is:

1. Determine expected C_D and C_L. Typical ranges for these quantities are $0.008<C_D<0.03$ and $0.2<C_L<0.5$. The actual values for these parameters are dictated by the choice of blade section shape, flow regime and the degree of blade section scaling.
2. Perform parametric design study using expected C_D/C_L to determine number of blades and tip speed ratio. A typical value for this ratio is 0.06.
3. Select a design point from the parametric study of step 2. The turbine design point is characterized by the number of turbine blades and the tip speed ratio. In general, the more blades that a turbine has the greater its efficiency. However, in actual application this must be balanced by the manufacture costs of the turbine.
4. Choose the turbine diameter, free stream flow speed and rotation rate consistent with the chosen tip speed ratio in step 3 above such that desired power is achieved. Maximum turbine diameter is dictated by the water depth and installation scheme where the turbine will operate. It is generally desirable to maximize the turbine diameter in order to maximize the turbine's power capacity. Free stream flow speed is determined by the flow where the turbine will be installed. Desired rotation rate will be effected by the electrical generator selected for use with the turbine.
5. Perform an off-design performance analysis. An off-design performance analysis is necessary to obtain an overall picture of the time average power that the turbine will produce. This analysis is especially important for tidal turbines where there is a fluctuation of flow speed.
6. Determine the span-wise blade chord and thickness distribution. This step is where the blade geometry is determined to produce the characteristics determined in the previous steps. OpenProp can perform this step automatically by using the chord optimizer.
7. Perform blade stress analysis. A blade stress analysis is necessary to ensure the structural adequacy of the blades.

The above procedure was used to design the turbine which was tested by Epps in Reference 6 and retested as part of this project with the exception of step 7. Step 7 was not performed as part of the design process because the stress module of OpenProp was not available at that time. The turbine diameter was selected as the maximum diameter which could be manufactured using the available rapid prototyping equipment and tested in the water tunnel test section. The number of blades was also dictated by the desire to maximize the turbine diameter and two blades were selected.

In Reference 6, Epps describes the procedure implemented in OpenProp to conduct a parametric design study, optimize a single turbine design and perform off design analysis. For turbines the method can be summarized as setting the blade circulation less than zero and then simultaneously solving a set of equations such that the resulting variables represent a physically realizable condition. Reference 6 also discusses the correct way to optimize a turbine design.

Once the turbine was designed, the geometry module of OpenProp was used to create the set of points that represent the blade surface in three dimensions. This set of points was loaded into SolidWorks® via a macro developed for this purpose. In SolidWorks®, the blade geometry was turned into a solid which was multiplied into two blades and attached to a hub. This file was saved in .stl format and loaded into the rapid prototyping machine for production. The model scale turbine that was generated in this way was tested by Epps in Reference 6 and as part of this project. Turbine test results are presented in the next section.

Table 9.1 of Reference 6 contains the turbine design parameters. That table is reproduced here in Table 2.

Parameter	**Value**	**Description**
Z	2	Number of blades
n	19.1 rev/s	Rotation rate
D	0.25 m	Diameter
V_s	3 m/s	Free stream speed
D_{hub}	0.08382	Hub diameter
M	20	Number of panels
ρ	1000 kg/m^3	Water density
λ	5	Tip speed ratio
$C_{L,max}$	0.5	Maximum allowable lift coefficient

Table 2: Key Turbine Parameters

Chapter 3 – Test Procedure, Results and Comparison

Test Procedure

Calibration

Calibration of the test fixture was performed by hanging known weights from the output shaft of the test fixture and reading strain gage amplifier output voltage using LabView®. This calibration technique is a static calibration; a better calibration technique for this type of testing would have been a dynamic calibration. However, a dynamic calibration is more complicated and requires additional equipment which was unavailable. LabView® was connected to the test fixture in an identical way for both calibration and testing. Results of the calibration are shown Figure 1 and Figure 2.

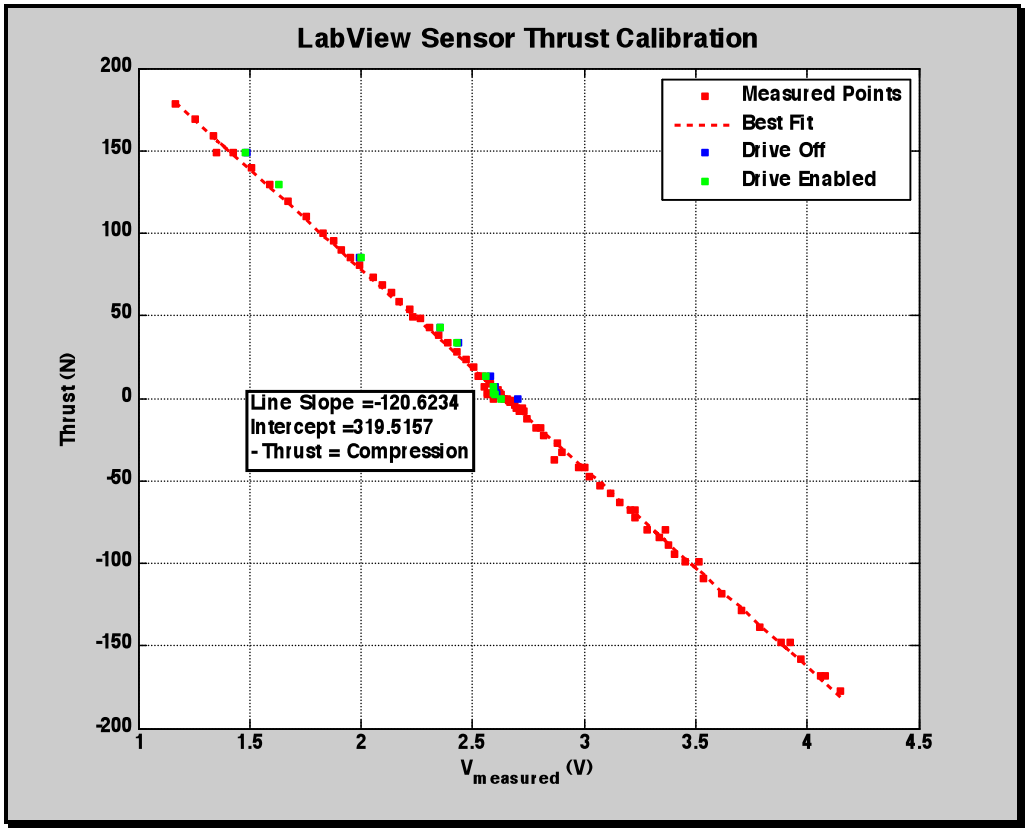

Figure 1: Thrust Calibration

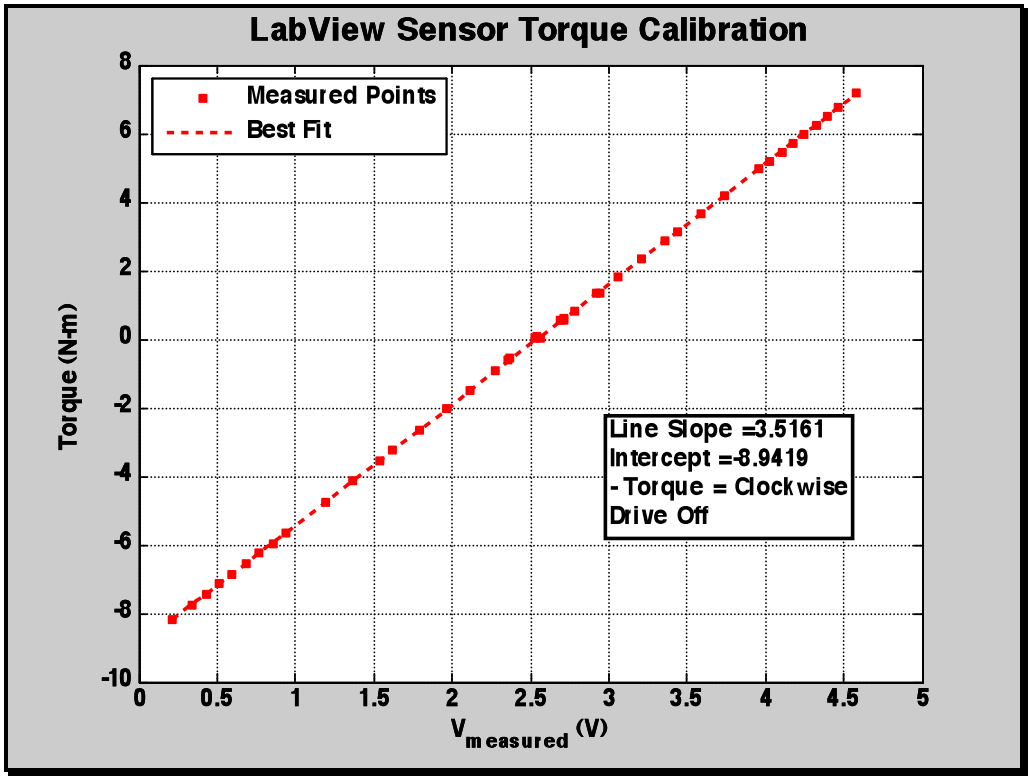

Figure 2: Torque Calibration

Because the motor drive used for these tests uses pulse width modulation (PWM) at 300VDC and because the signal wires are running alongside the power cable (inside the same 1.5 inch diameter standpipe) there was a concern that the Signal to Noise Ratio (SNR) would be too small to be able to effectively measure the signal voltage. This concern was allayed by performing spectral analyses on the measured signal. A typical result of these analyses is shown in Figure 3. The graph shows that there is minimal interference.

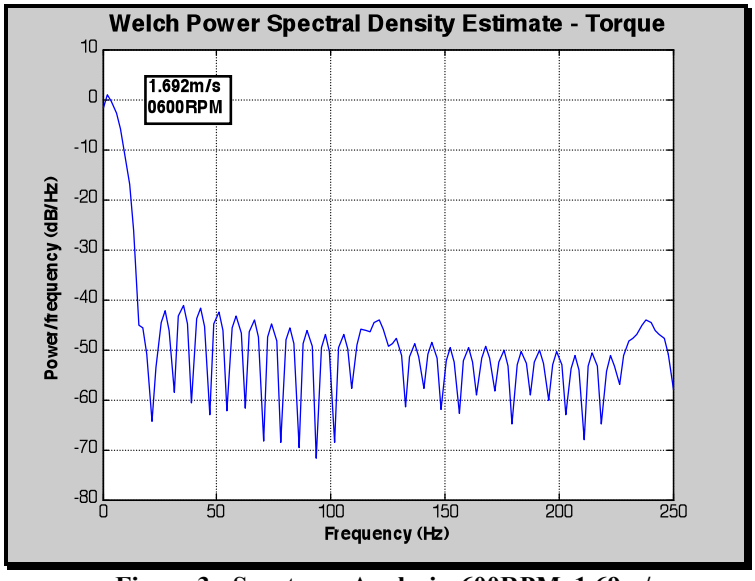

Figure 3: Spectrum Analysis–600RPM, 1.69m/s

Since the calibration that was used was a static calibration, it is necessary to correct the measured torque with the friction torque in order to determine the actual torque produced by the turbine. A graph of friction torque measured at various rotation rates without a hub or turbine attached, but with the test fixture submerged in the test section, is given in Figure 4. These values are used to correct the torque measured by the sensor.

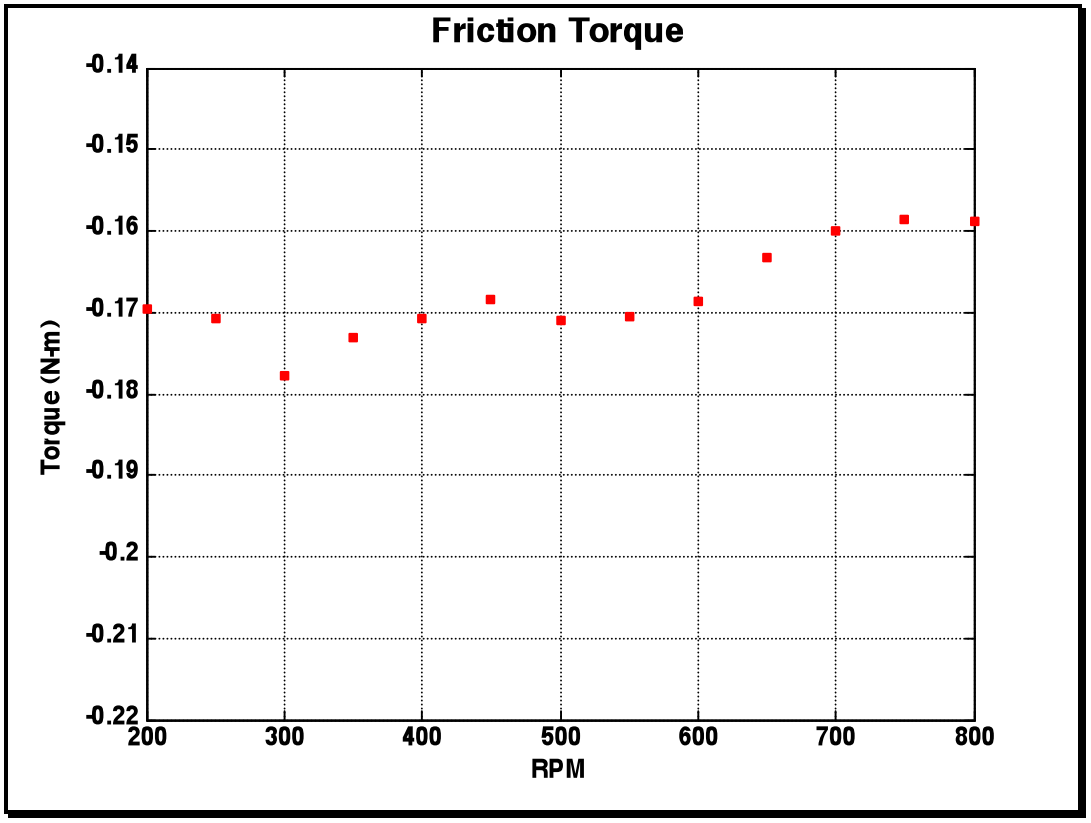

Figure 4: Friction Torque

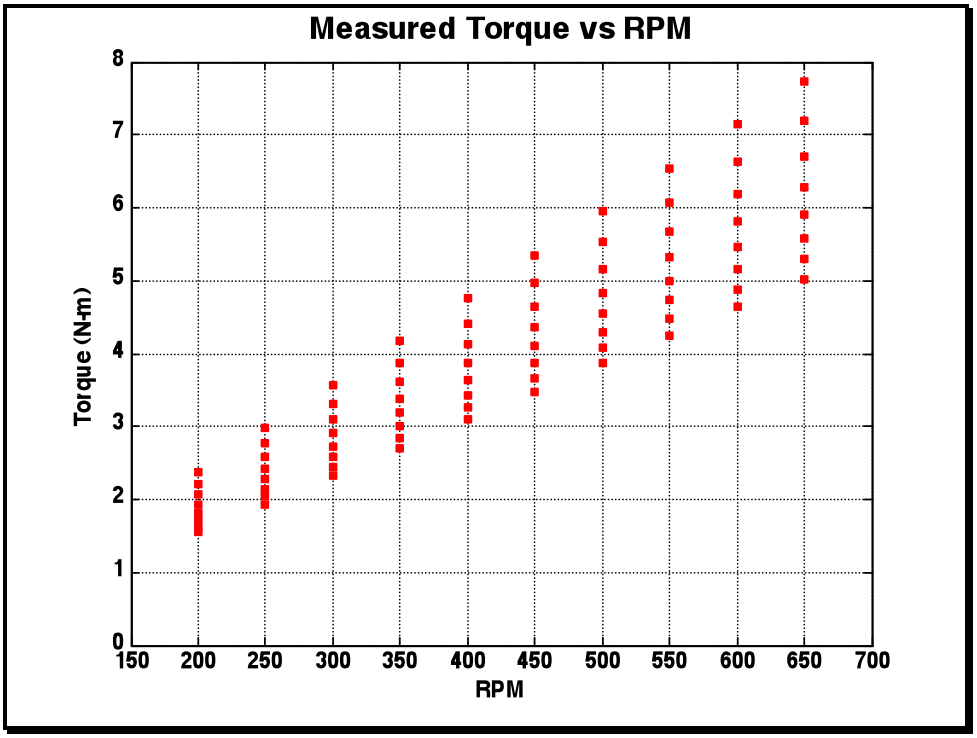

Figure 5: Measured Torque – No Correction

Figure 5 shows the torque measured by the sensor without torque correction. Comparison of Figure 4 and Figure 5 shows that the friction torque is a relatively small value compared to the total measured torque.

Test Steps

Testing began by determining the tip speed ratios that would bracket the turbine's design point and reproduce the entire off design performance curve generated by OpenProp. The tip speed ratios which were used in this test are shown in Table 3.

Tip Speed Ratio - λ										
		RPM								
		200	**250**	**300**	**350**	**400**	**450**	**500**	**550**	**600**	**650**
Flow Speed (m/s)	**1.100**	2.38	2.97	3.57	4.16	4.76	5.35	5.95	6.54	7.14	7.73
	1.185	2.21	2.76	3.31	3.87	4.42	4.97	5.52	6.08	6.63	7.18
	1.269	2.06	2.58	3.09	3.61	4.13	4.64	5.16	5.67	6.19	6.70
	1.354	1.93	2.42	2.90	3.38	3.87	4.35	4.83	5.32	5.80	6.28
	1.438	1.82	2.28	2.73	3.19	3.64	4.10	4.55	5.01	5.46	5.92
	1.523	1.72	2.15	2.58	3.01	3.44	3.87	4.30	4.73	5.16	5.59
	1.608	1.63	2.04	2.44	2.85	3.26	3.66	4.07	4.48	4.89	5.29
	1.692	1.55	1.93	2.32	2.71	3.09	3.48	3.87	4.25	4.64	5.03

Table 3: Test Tip Speed Ratios

The steps taken to gather the data displayed in Figure 7 are outlined below:

1. Generate Table 3 which represents the test points at which data was gathered. Flow speeds selected correspond to integer speed reference number increments of Figure 6
2. Set water tunnel impeller speed to create desired flow speed in test section
3. Command desired test fixture motor rotation
4. Collect torque and voltage measurements via the LabView® interface. Sample rate was set at 500Hz. Sample time was 5-10 seconds.
5. Increase test fixture motor rotation rate
6. Wait approximately 10 seconds for transient behavior to subside
7. Repeat steps 4-6 until data has been collected for every rotation rate at the test section flow speed
8. Increase test section flow speed
9. Wait approximately one minute for transient behavior to subside.
10. Repeat steps 3-9 until all data has been collected.

Conducting the test in the order listed above minimizes the time required to collect data since the transient is much longer for a water tunnel impeller speed change than for a test fixture motor speed change.

In step 2, the water flow speed in the tunnel was not measured directly. Normal mode of operation is to measure the flow speed in the test section using a Laser Doppler Velocimetry (LDV) system; however the LDV system was not operational at the time of the test. Previous experimentation in the water tunnel generated Figure 6. Figure 4 relates impeller rotation rate to test section flow speed. This data was gathered using a PIV flow measurement technique with a trolling motor test apparatus in the test section. The trolling motor provides similar test section blockage as the test fixture described herein. Note that the speed reference number in Figure 6 corresponds to the output frequency from the impeller motor drive to the impeller motor.

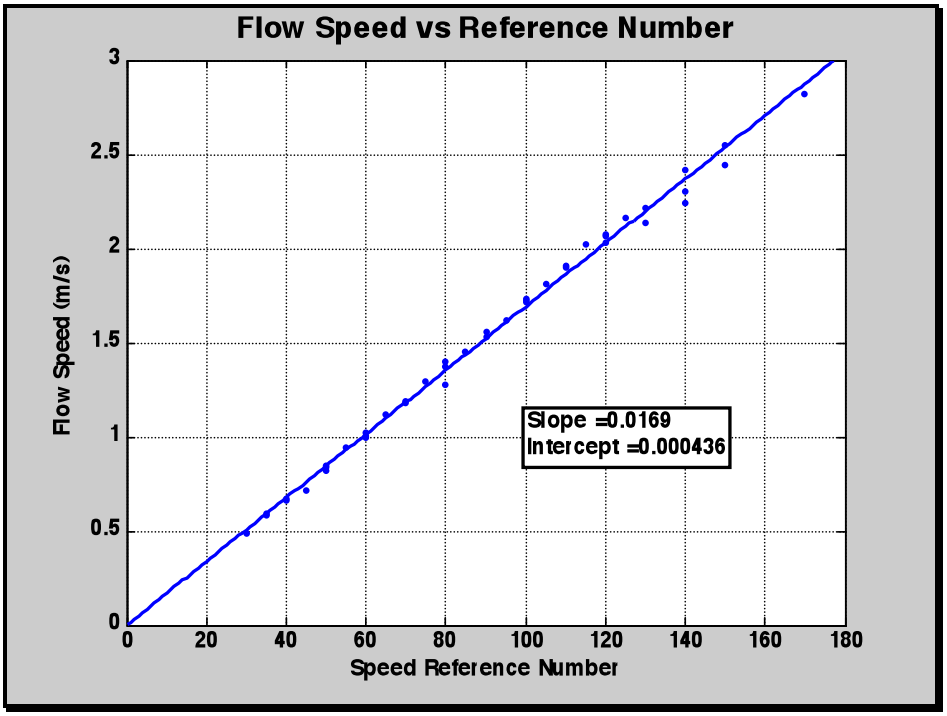

Figure 6: Test Section Flow Speed Determination

Step 3 was accomplished by operating the test fixture motor drive in the programmed velocity mode via the ASCII command line of the Copley Motion Explorer (CME) software. In the programmed velocity mode, a rotation speed is commanded and the motor drive maintains this speed regardless of the direction of energy flow. For this test the motor is acting as a generator being held at the commanded rotation rate. In the command window of CME it was observed that the RPM was being held to the commanded RPM +/- 2-3 RPM.

Results and Comparison

The results of the test are shown in Figure 7.

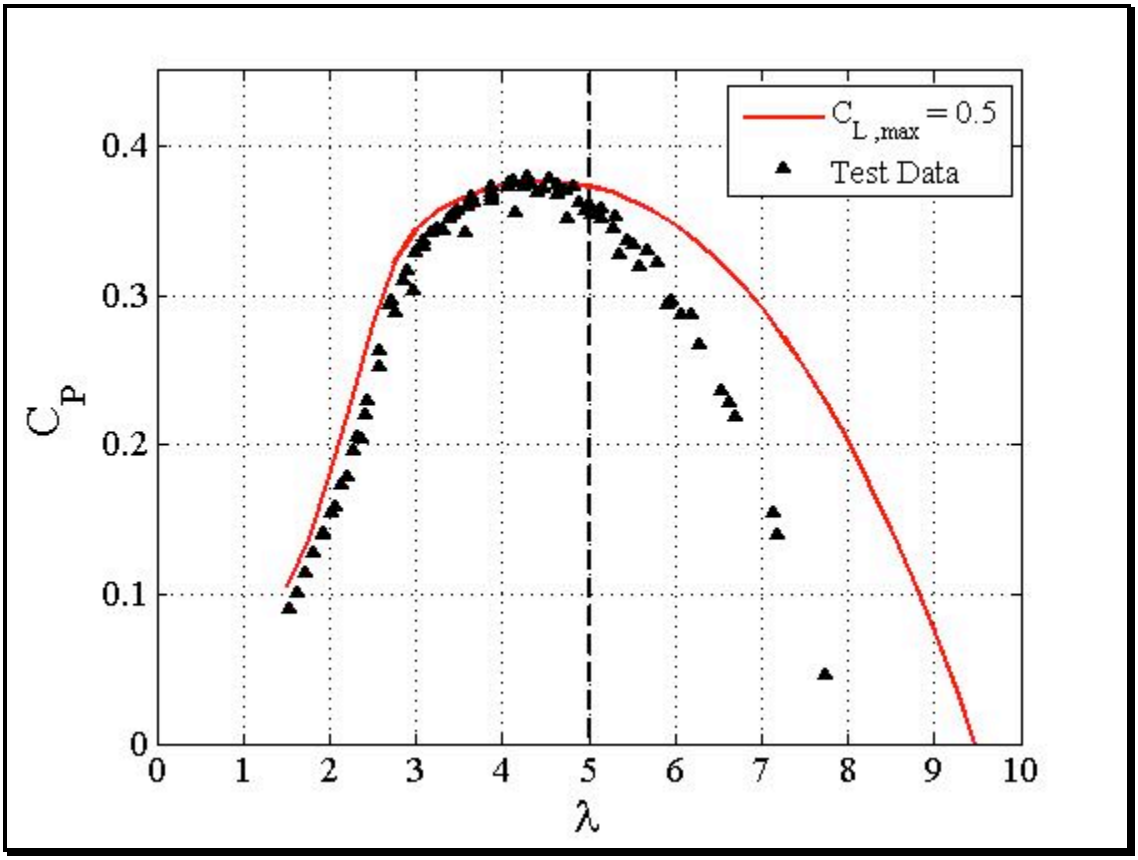

Figure 7: Results

Figure 7 shows the following:

1. There is good agreement between predicted and experimental data for tip speed ratios (λ) less than 5.
2. On design predicted performance almost exactly matches the experimental on design performance.
3. Experimental and predicted performance diverge for λ greater than 5.

As a result of the experimental results shown in Figure 7, OpenProp is being revised to more accurately predict performance for λ greater than λ_{Design}. It is thought that the divergence can be accounted for by implementing a more sophisticated model of bound and free circulation via lifting surface methods. This is a point of ongoing work in OpenProp.

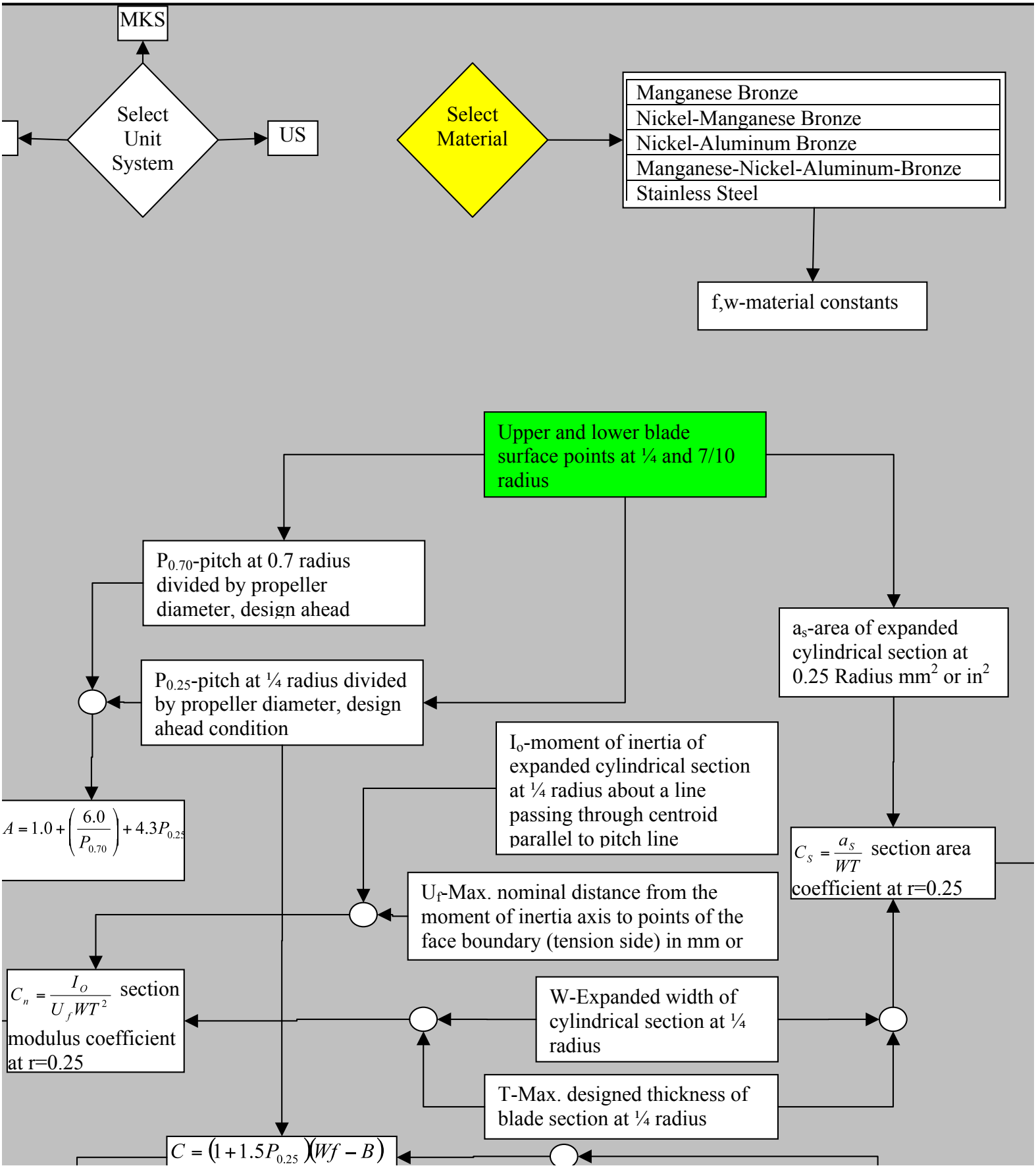
MKS
Select Unit System
US
Select Material
Manganese Bronze
Nickel-Manganese Bronze
Nickel-Aluminum Bronze
Manganese-Nickel-Aluminum-Bronze
Stainless Steel
f,w-material constants
Upper and lower blade surface points at ¼ and 7/10 radius
P0.70-pitch at 0.7 radius divided by propeller diameter, design ahead
as-area of expanded cylindrical section at 0.25 Radius mm2 or in2
P0.25-pitch at ¼ radius divided by propeller diameter, design ahead condition
Io-moment of inertia of expanded cylindrical section at ¼ radius about a line passing through centroid parallel to pitch line
$A = 1.0 + \left(\frac{6.0}{P_{0.70}}\right) + 4.3P_{0.25}$
$C_S = \frac{a_S}{WT}$ section area coefficient at r=0.25
Uf-Max. nominal distance from the moment of inertia axis to points of the face boundary (tension side) in mm or
$C_n = \frac{I_O}{U_f WT^2}$ section modulus coefficient at r=0.25
W-Expanded width of cylindrical section at ¼ radius
T-Max. designed thickness of blade section at ¼ radius
$C = (1 + 1.5P_{0.25})(Wf - B)$

This section describes the implementation of the American Bureau of Shipping (ABS) steel vessel rules into OpenProp as a first attempt in the design process to check the adequacy of the blade dimensions and material to support the loads they will carry. The output of OpenProp blade structure code is a check of the blade thickness at the quarter span section against the required blade thickness at the quarter span section as determined from implementation of the steel vessel rules. While the steel vessel rules do not actually calculate a stress or determine the operational lifetime of a propeller they do take these quantities into consideration as evidenced by the requirement written into the rules to qualify a material other the those listed above for service in a classed vessel. The rules also represent what is required in order to class a vessel with any of the many classification societies worldwide.

Rule Implementation in OpenProp

The OpenProp module which implements the ABS rules for propellers does so in a way which follows the flowchart shown in the figure above. User input for this module is only the material that is being used for the propeller construction. ABS lists five different materials that can be used for propeller manufacture; these are listed in the flowchart above. The lines of code which correspond to the desired material must be uncommented in order to use that material in the calculations performed. All other required input for implementation of the rules is automatically extracted from other modules of OpenProp or calculated within the blade structure module. User input is highlighted in yellow; input from other modules is highlighted in green. Since other OpenProp modules use the SI unit system, the user is not allow to select a different unit system. The output of the structure module is a small table which lists the section thickness at the quarter span section and the required section thickness at the quarter span section, as calculated from the ABS rules. Propeller redesign is necessary if the required blade thickness is greater than the design blade thickness.

Limitations

In its current version OpenProp designs fixed pitch, single propellers and turbines without rake or skew. The ABS rules for propellers allow for controllable pitch, rake and skew but the structure module developed as part of this project only performs the calculations for fixed pitch, single propellers without rake or skew. The rules used to develop the code of this project do not cover contra-rotating propellers, ducted propellers or propellers for vessels in ice. Additional structure module capability could easily be added at a later date to incorporate the ever increasing capabilities of the OpenProp.

Moment of Inertia Calculation

The bulk of the code to implement the ABS rules for propellers is used to determine the moment of inertia of the designed propeller quarter span blade section. The blade structure module of OpenProp imports the points from the pressure and suction sides of the quarter span section. All of the points are then shifted so that the points lie in the first quadrant of the x-y plane. Shifting the points makes the determination of the quarter span section neutral axis easier. The code then performs a trapezoidal integration for the pressure and suction sides separately and subtracts the area of the pressure side from the suction side so that only the section area remains. The moment of inertia about the x-axis is then calculated and the parallel axis theorem used to find the moment of inertia about the neutral axis. A flowchart of the portion of the code which calculates the moment of inertia is shown in the figure below.

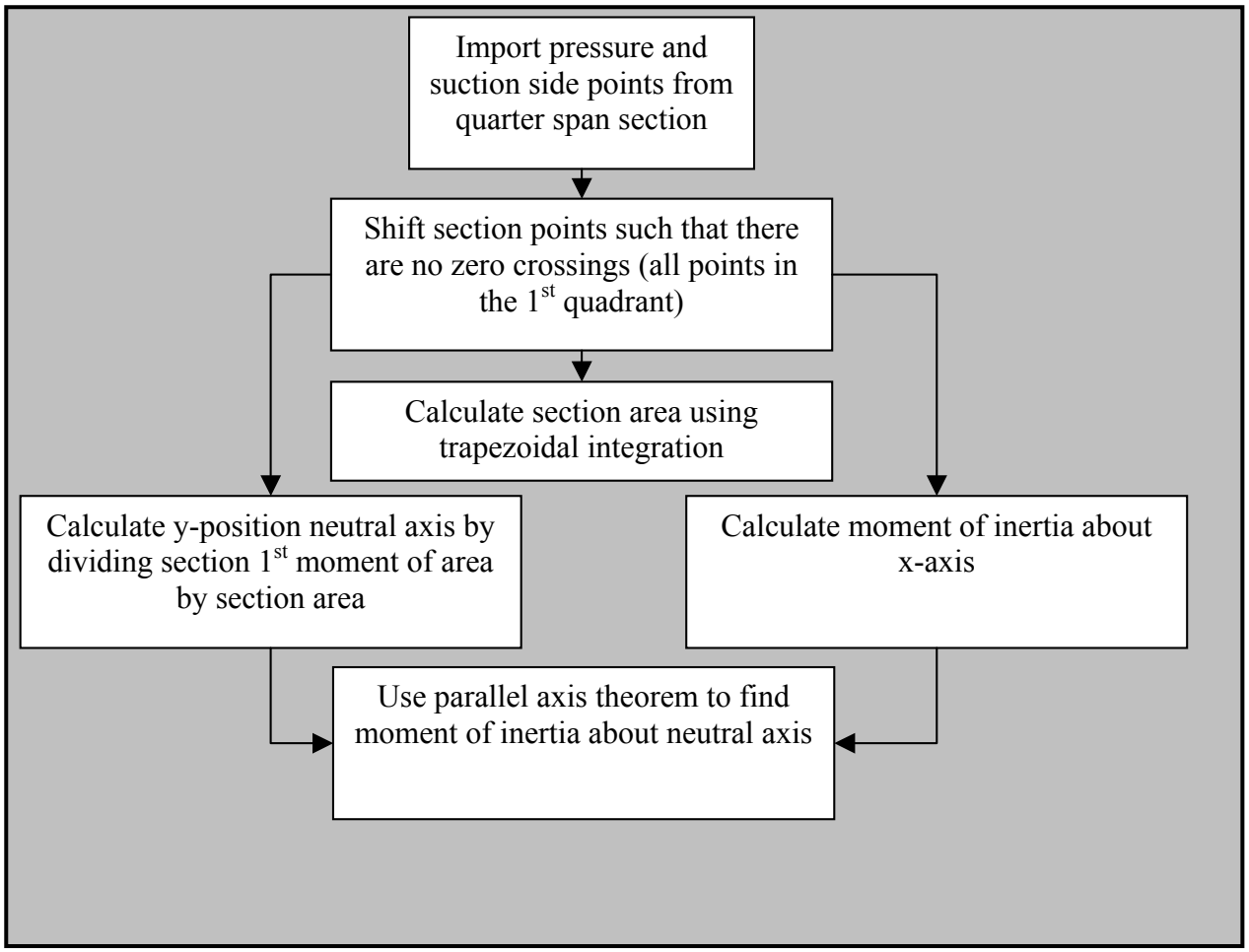

Figure 2: Code Flowchart to Find Section Area and Moment of Inertia

Chapter 5 – Calculation of Blade Stress

Theory

A relatively simple method to estimate the stress on a propeller blade is to implement beam bending theory. The derivation given below is an amplification of the derivation presented in Reference 10. Reference 10 also includes some historical background for this method. The basic assumptions of the derivation are:

1. The blade acts as a cantilevered beam.
2. Axial stresses are due to bending and centrifugal forces.
3. Sheer stresses are negligible.

Figure 8 below shows a propeller blade section with the associated inflow velocities and lift force. By definition the lift force, *dL*, is always perpendicular to the total inflow velocity V^*. *dL* is responsible for both thrust and torque on the propeller blades and propeller shaft.

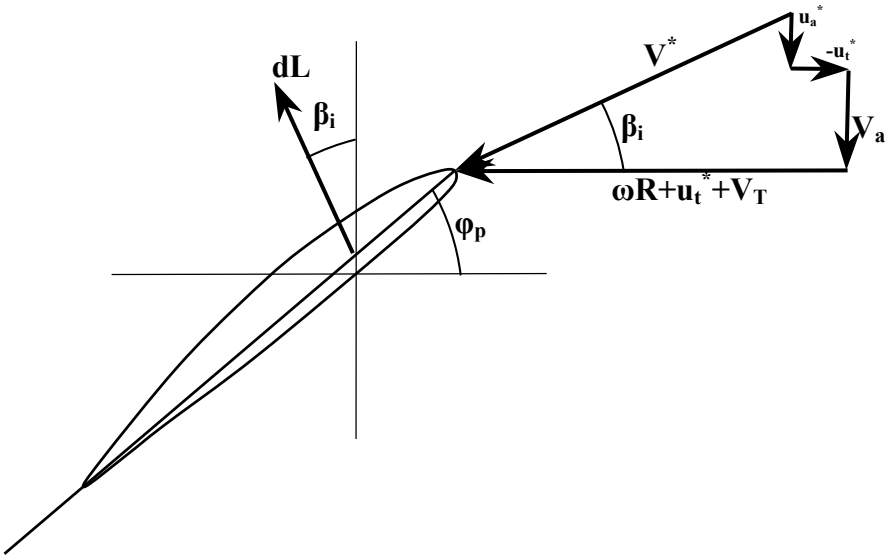

Figure 8: Blade Section with Lift and Flow Velocity Vectors

Note that *dL* is always perpendicular to V^* but its typically not perpendicular to the chord line. Therefore, when determining the component of *dL* that produces thrust and the component of the *dL* which produces torque, the inflow angle β_i is required, not the blade pitch angle, φ_p. The elemental lift at a blade section is given by Equation 1.

$$dL = \frac{1}{2}\rho (V^*)^2 C_L c dr \quad \mathbf{1}$$

where
dL = elemental lift on a blade section
ρ = fluid density
C_L *= section lift coefficient at radius r, this comes from the lifting line calculation in OpenProp.*
c = section chord length at r
dr = elemental radial span

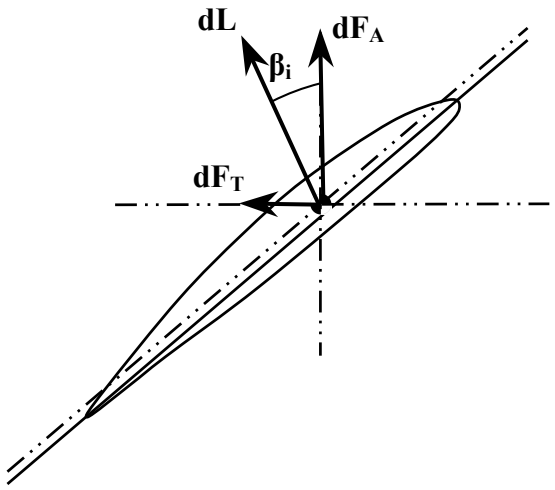

Figure 9: Blade Section Showing Lift Resolved into Axial and Tangential Components

From Figure 2, it can be seen that the axial force, F_A, and tangential force, F_T, at a blade section are given by:

$$dF_A = dL\cos(\beta_i + \varepsilon) \quad \mathbf{2}$$
$$dF_T = dL\sin(\beta_i + \varepsilon) \quad \mathbf{3}$$

where
β_i = *inflow angle*
$\varepsilon = C_D/C_L$, *inflow angle correction due to viscous effects*
C_D = *section drag coefficient*

Note that in Figure 9, the point of application of *dL* has been shifted to the centroid of the section and is no longer located at the same point as in Figure 8. This is done to simplify calculations. *dL* will not necessarily be located at the section centroid but at a point approximately ¼ of the distance from the leading edge to trailing edge on the chord line as shown in Figure 8. The fact that *dL* does not act through the section centroid means that *dL* will produce a torque about the span line of the blade. This torque and its associated sheer stress are assumed to be negligible along with all other shear stresses.

Both F_A and F_T produce bending moments about the centroidal axes. Each of these bending moments, along with their *x* and *y* components, is shown in Figure 10. The equations for the bending moment are:

$$dM_A = (r - r_o)\,dF_A \quad \mathbf{4}$$
$$dM_T = (r - r_o)\,dF_T \quad \mathbf{5}$$

where
r_o = *section radius where dM is being calculated*
r = radius of section producing lift

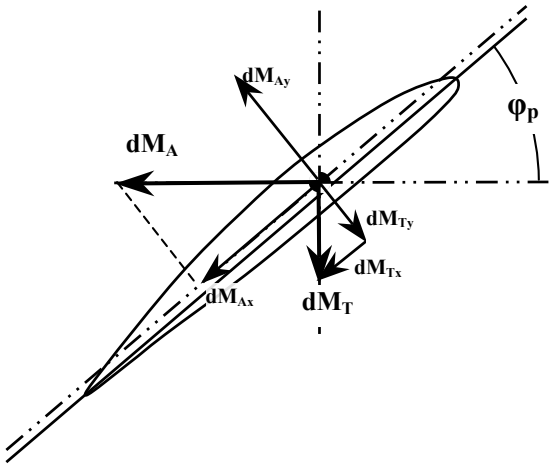

Figure 10: Bending Moments Components

The total moments produced by F_A and F_T, at a section r_o, are given by:

$$M_A = \int_{r_o}^{R} \frac{1}{2} \rho (V^*)^2 C_L c \cos(\beta_i + \varepsilon)(r - r_o)\, dr \quad \mathbf{6}$$

$$M_T = \int_{r_o}^{R} \frac{1}{2} \rho (V^*)^2 C_L c \sin(\beta_i + \varepsilon)(r - r_o)\, dr \quad \mathbf{7}$$

Because it is necessary to project these bending moments onto the centroidal axes of the section, blade pitch angle is required. Projecting the total bending moments onto the centroidal axes, the equations become

$$M_{X_o} = M_A \cos(\varphi_P) + M_T \sin(\varphi_P) \quad \mathbf{8}$$

$$M_{Y_o} = M_A \sin(\varphi_P) - M_T \cos(\varphi_P) \quad \mathbf{9}$$

Each of these bending moment vectors is shown in Figure 11

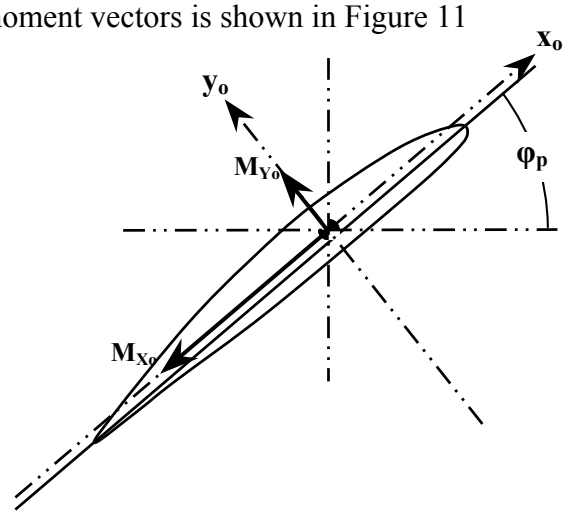

Figure 11: Total Bending Moments about Centroidal Axes

Additionally, the centrifugal force acting at each section contributes to the overall stress at the section. The elemental centrifugal force acting on a blade from an adjoining section is given by

$$dF_C = (2\pi n)^2 \, r \, dm \quad \textbf{10}$$

where
dm = $\rho_b A dr$ = mass of blade element
ρ_b = propeller blade material density
A = section area
c = section chord length
t = section thickness

Summing the contributions of all adjoining sections to the F_C at the section of interest, the total F_C at the section becomes

$$F_C = (2\pi n)^2 \rho_b \int_{r_o}^{R} A \, r \, dr \quad \textbf{11}$$

Since the blades analyzed using the above method do not contain rake or skew, which would introduce additional bending moments from F_C, the equation for the stress on a blade section can be expressed as:

$$\sigma = \frac{-M_{X_o} y}{I_{X_o}} - \frac{M_{Y_o} x}{I_{Y_o}} + \frac{F_C}{A} \quad \textbf{12}$$

Implementation

In order to implement the equations above it is necessary to calculate the required blade section quantities. Figure 12 and Figure 14 illustrate to overall procedure for determining 2D blade section area, centroid and moments of inertia.

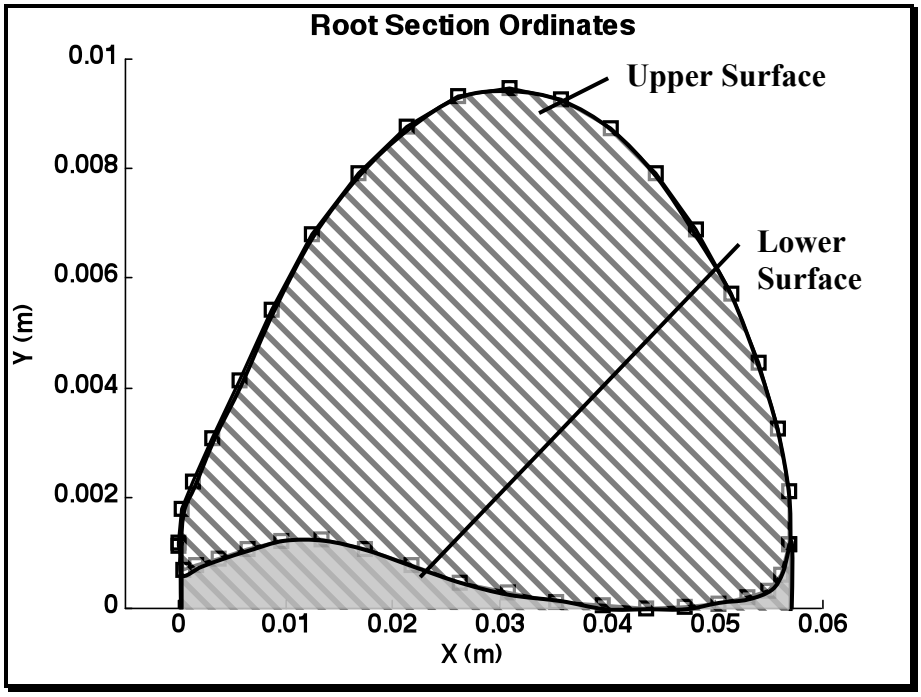

Figure 12: Distorted Root Section

Figure 12 shows the visually distorted root section of the propeller whose design is describe in Reference 6. The section is distorted for illustrative purposes. OpenProp treats the blade section as composed of an upper and lower surface. The overall procedure for determining blade section area properties was to determine the area properties of the area formed by the uppers surface and the x-axis and subtract the area properties formed by the lower surface and the x-axis. This subtraction results in the properties of the enclosed area shown above.

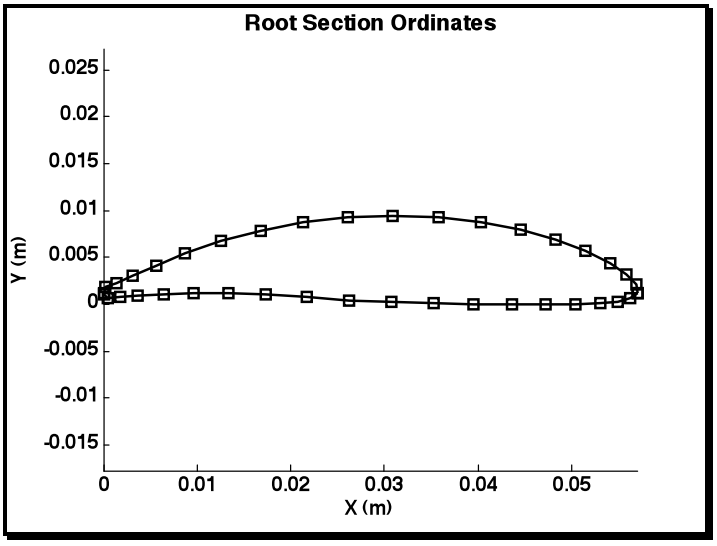

Figure 13: Undistorted Root Section

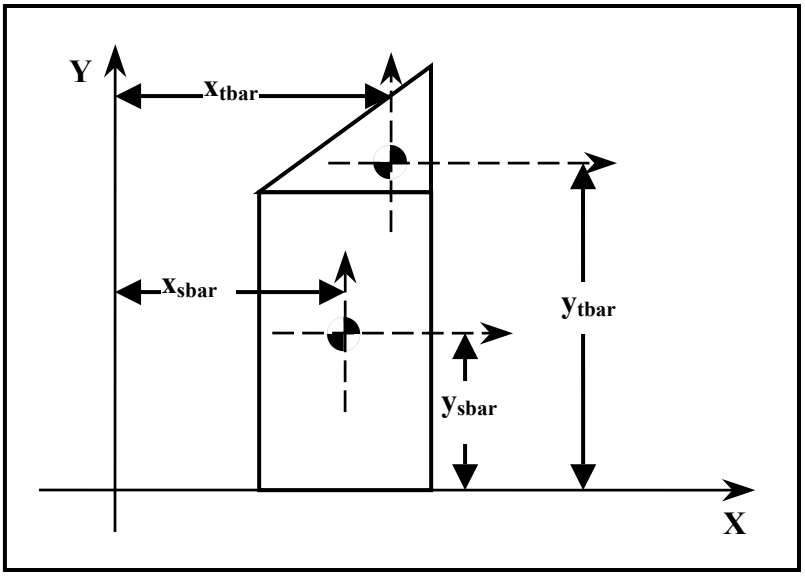

Figure 14: Calculation of Elemental Area Properties

Figure 14 shows a characteristic diagram that was used to determine elemental area properties which were summed to achieve the section area properties. The procedure was:

1. Determine elemental area
2. Calculate elemental centroid
3. Calculate elemental 2nd moment of area about both x and y axes
4. Sum elemental areas
5. Sum 2nd moment of areas about x and y axes
6. Calculate section centroid, Equation 13

$$\bar{Y} = \frac{\sum \bar{y}_i A_i}{\sum A_i}, \; \bar{X} = \frac{\sum \bar{x}_i A_i}{\sum A_i} \quad \textbf{13}$$

7. Apply parallel axis theorem to determine 2nd moment of area about the centroidal axes, Equation 14.

$$I_{Centroid\,X} = I_X - \bar{Y}^2 A_{total}, \; I_{Centroid\,Y} = I_Y - \bar{X}^2 A_{total} \quad \textbf{14}$$

In order to determine the other quantities required by Equation 12, the integrals were turned into discrete sums and variables from the propeller design were used.

Results

The results of the analysis performed for the propeller described in Reference 6 are shown below for an on design and off design condition. Figure 15 shows the stress at the blade root. As expected, the blade is in tension on the pressure side and compression on the suction side. Note that the stresses indicated in Figure 15 in the middle of the root section are interpolated stress. Only the stresses at the blade surface were calculated at the points indicated.

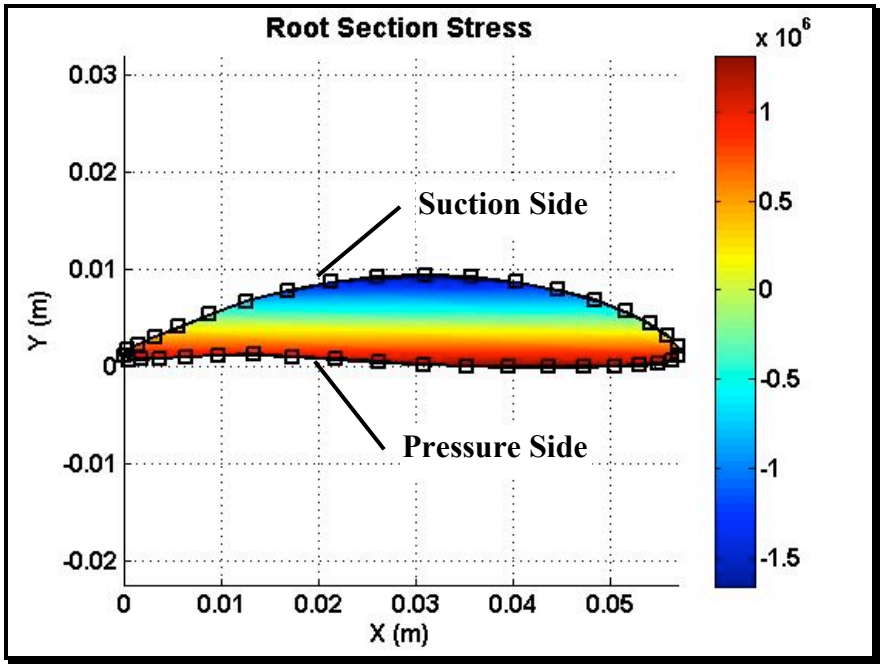

Figure 15: On Design Root Section Stress

In Figure 16 through Figure 19 tensile stresses are considered positive and compressive stresses negative. Figure 16 and Figure 17 represent the on design condition while Figure 18 and Figure 19 represent an off design condition as specified the figure titles. As expected the off-design condition chosen shows higher stresses than the on-design condition. This is a result of selecting an off design condition where both K_T and K_Q are higher than on-design. This means that the propeller is creating greater thrust and torque in the off-design condition which results in higher stress.

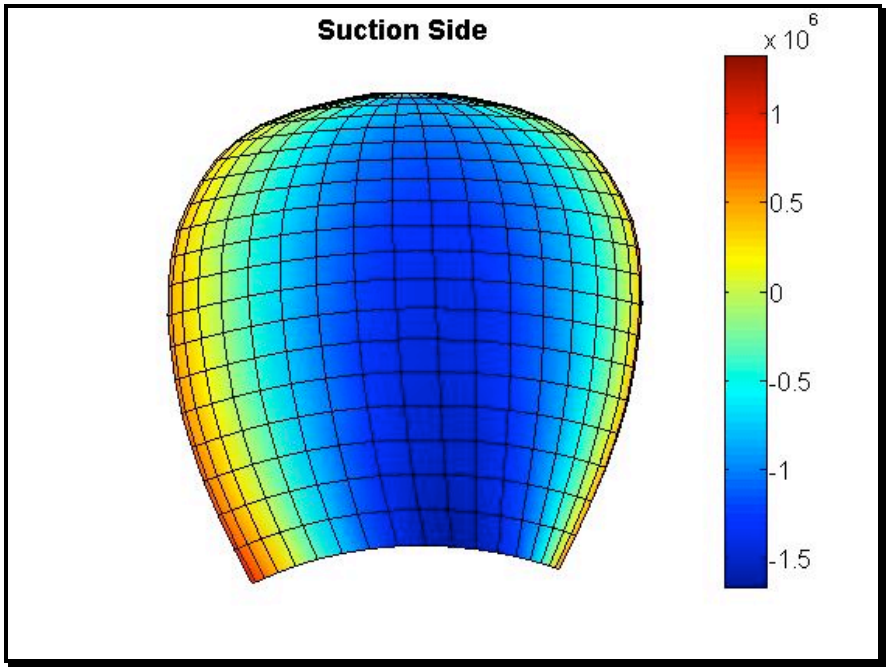

Figure 16: On Design Suction Side Stress: *J_s=0.75, V_S=1.5m/s, n=8rev/s, D=0.25m*

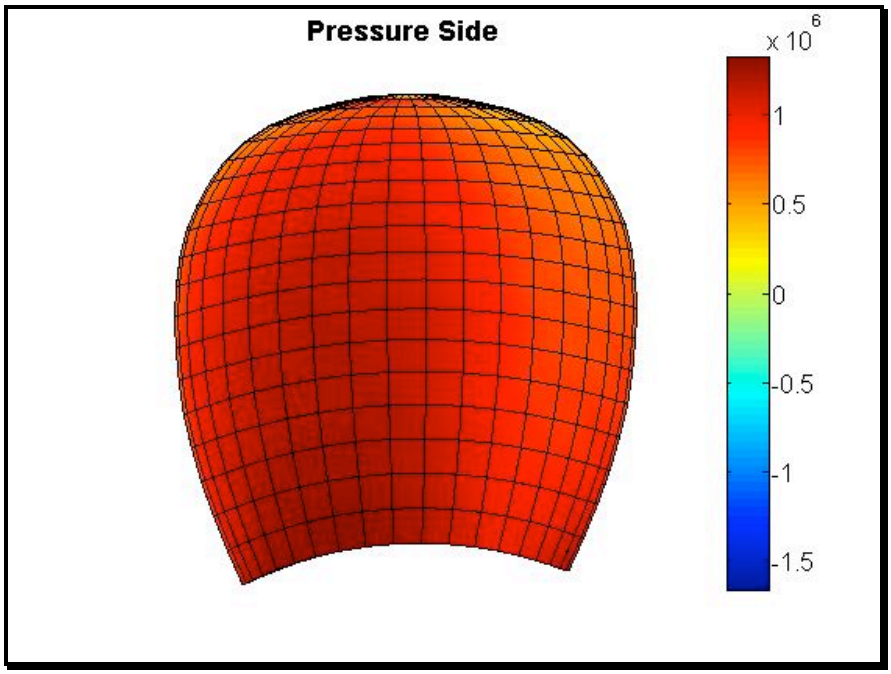

Figure 17: On Design Pressure Side Stress: *J_s=0.75, V_S=1.5m/s, n=8rev/s, D=0.25m*

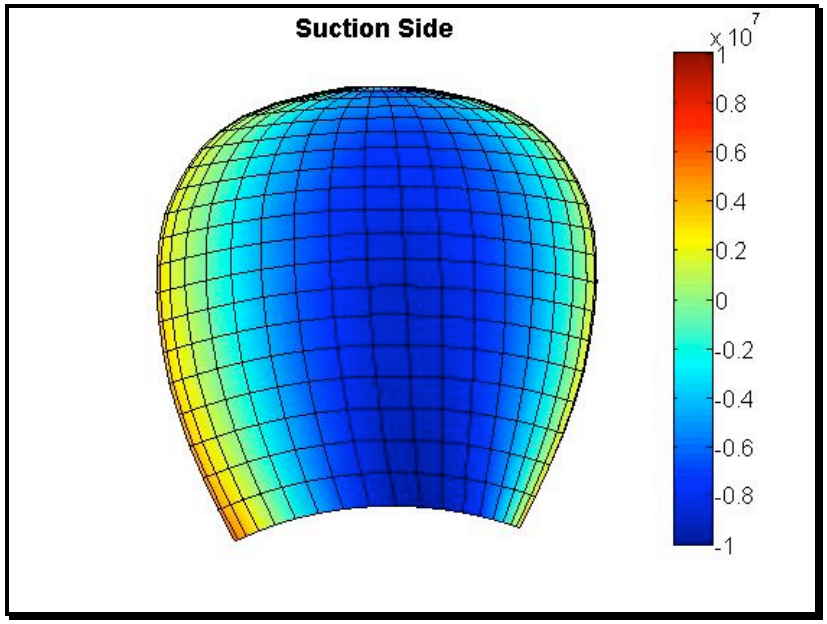

Figure 18: Off Design Suction Side Stress: *J_s=0.40, V_S=1.5m/s, n=15rev/s, D=0.25m*

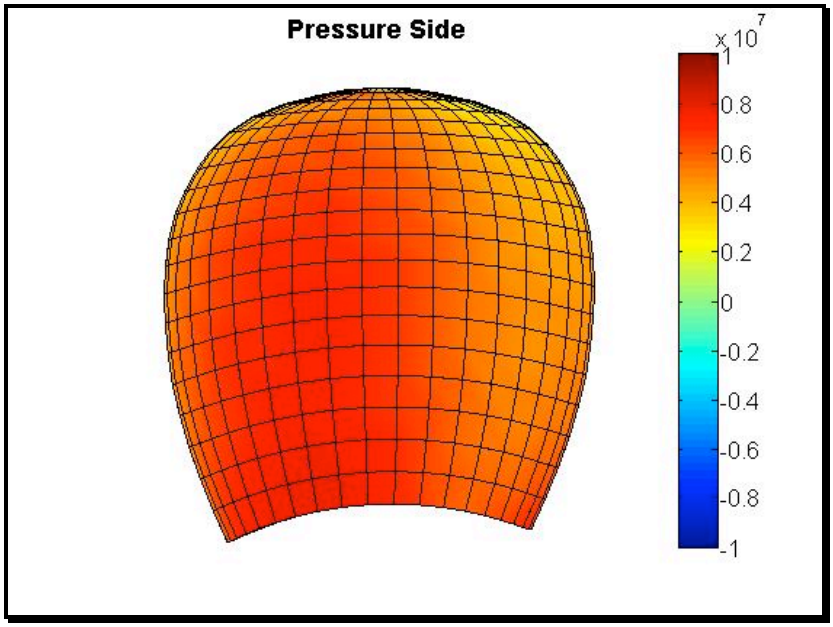

Figure 19: Off Design Pressure Side Stress: *J_s=0.40, V_S=1.5m/s, n=15rev/s, D=0.25m*

Carlton presents isostress contour lines taken from FEA results for various propeller types in Reference 2. The results presented above agree with the trends presented by Carlton for a propeller blade without skew. Carlton shows highest stress near the blade mid-chord in a region that extends close to the tip of the blade and a decreasing stress as one moves away from the mid-chord to the blade leading and trailing edges.

Chapter 6 – Fatigue Analysis

By definition fatigue failure is characterized by a time varying load whose magnitude is smaller than that required to produce failure in a single application. The fatigue analysis conducted as part of this project is presented in two steps.

1. Identification of the cyclic loading
2. Application of a fatigue failure theory.

A comprehensive fatigue analysis is characterized by many subtleties and in many cases significant experience is necessary to conduct the art of a fatigue analysis. The fatigue analysis presented here is intended to provide a method by which a fatigue analysis could be conducted on a propeller or turbine at the beginning of the design process to ensure the estimated fatigue life meets the design goal. As a whole, OpenProp is intended to be a design tool which can be used to provide good initial propeller and turbine designs. As additional iterations of the design process are completed more sophisticated tools for propeller design will become necessary. It is in this spirit of providing good initial design estimates that the fatigue analysis is presented here.

Cyclic Load

For a propeller or turbine the source of the varying load is the wake that it operates in. Due to the presence of a wake, the inflow velocities to the blades are not uniform in magnitude or direction. As a blade completes a revolution it will pass through regions of various velocity which will induce varying forces on the blade. A propeller will typically operate in a wake with greater inflow velocity variation than a turbine. Because a propeller operates in a more severe wake environment and because wake data is more readily available for propellers, fatigue analysis for a propeller was performed.

A wake for a single screw ship is shown in Figure 20. This figure clearly shows a circumferential variation in the axial inflow velocity. Typically there is also a circumferential variation in the tangential inflow velocity but this variation is much smaller and is not considered here. This is shown in wake profiles of Reference 8. Figure 20 shows the ship wake divided into twelve sectors. As the blade passes through each sector it is assumed to fully develop its lift commensurate with the flow velocity in that sector. This assumption makes this analysis a quasi-steady analysis. In each sector, the circumferential average of the axial inflow velocities was taken at the same radial positions that were used in the propeller design. Each blade section is subjected to a different inflow velocity which results in a different C_L. In order to determine the new C_L on each section Equation 1 was used.

$$C_{Lf} = C_{Lo} + 2\pi(\Delta\alpha) \quad \textbf{15}$$

where
C_{Lo} = original lift coefficient in the design condition
C_{Lf} = new lift coefficient at the new angle of attack
$\Delta\alpha$ = change in angle of attack from design condition

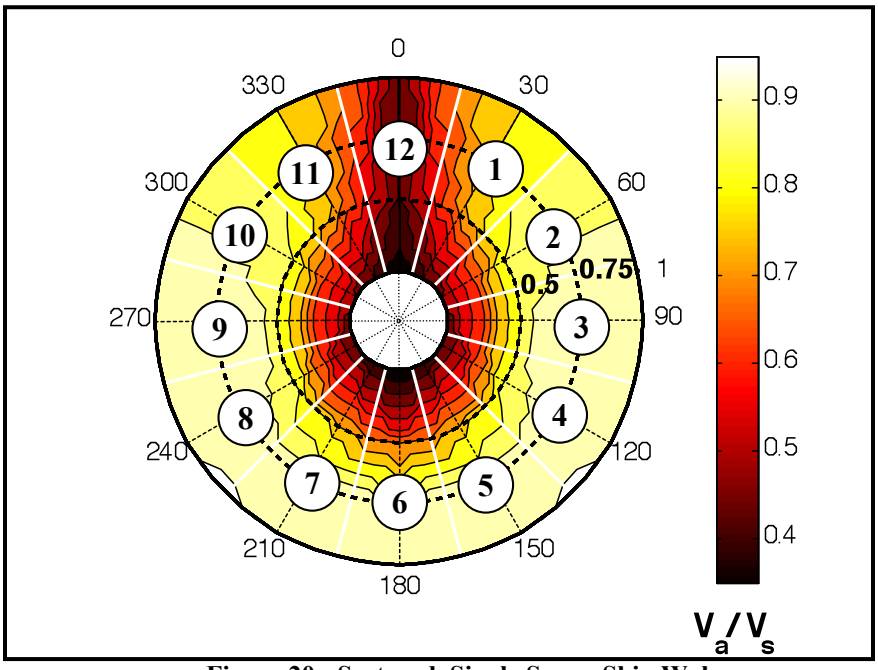

Figure 20: Sectored, Single Screw Ship Wake

Figure 21 and Figure 22 show how a change in the axial velocity produces a change in the magnitude and direction of the total inflow velocity. The analysis also assumes that u^*_a and u^*_t remain constant.

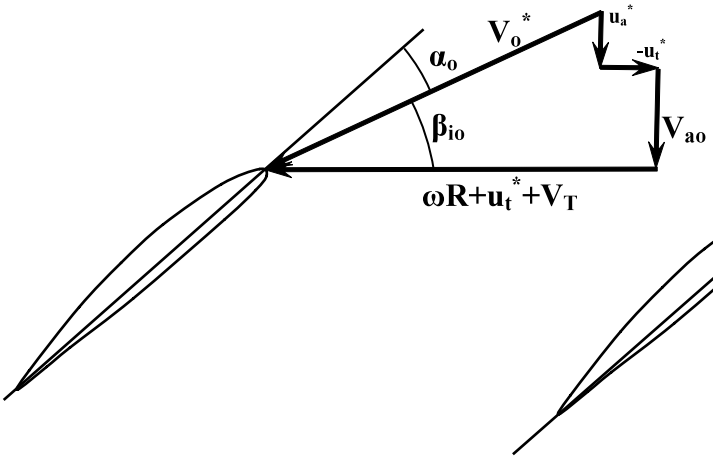

Figure 21: Original Inflow Velocities

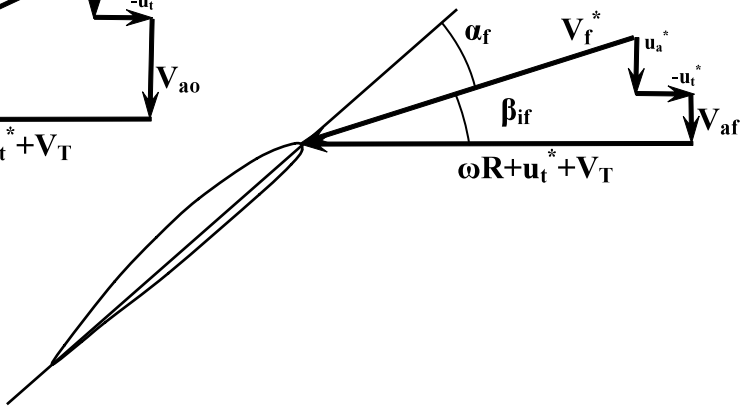

Figure 22: New Inflow Velocities

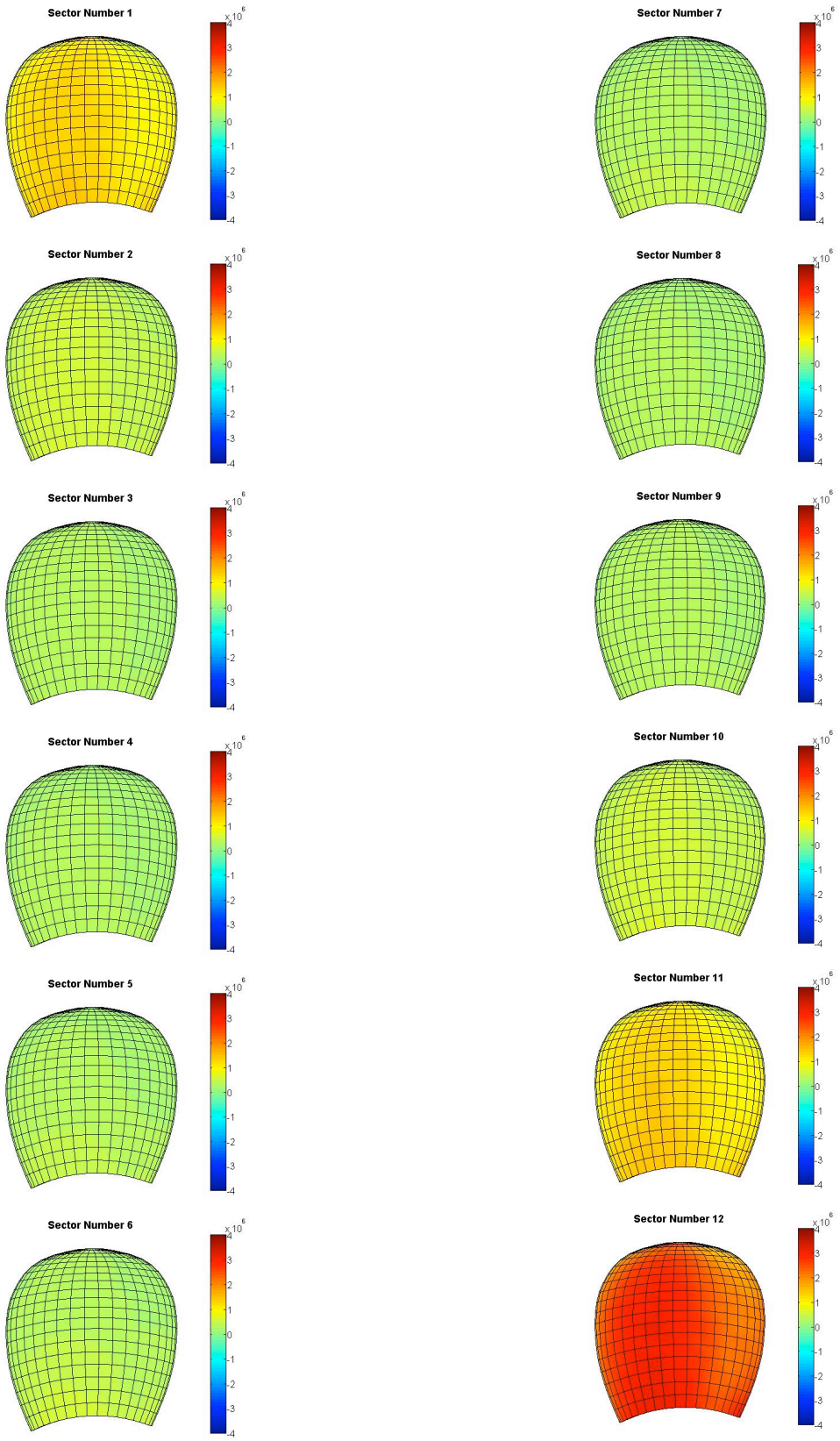

Figure 23: Pressure Side Blade Stress for Each Wake Sector

Figure 23 above shows the change in blade stress as the blade passes through the wake sectors of Figure 20. As expected, the highest stresses occur in sector number twelve where the axial inflow velocity is the lowest. The lowest axial inflow produces the largest angle of attack and lift coefficient and subjects the blade to the largest amounts of lift force and stress.

Since the blade stress varies considerably across the blade faces, it is necessary to identify the point where maximum tensile stress occurs. The point of maximum stress for this propeller occurs at the blade root at the point identified by the arrow in Figure 24.

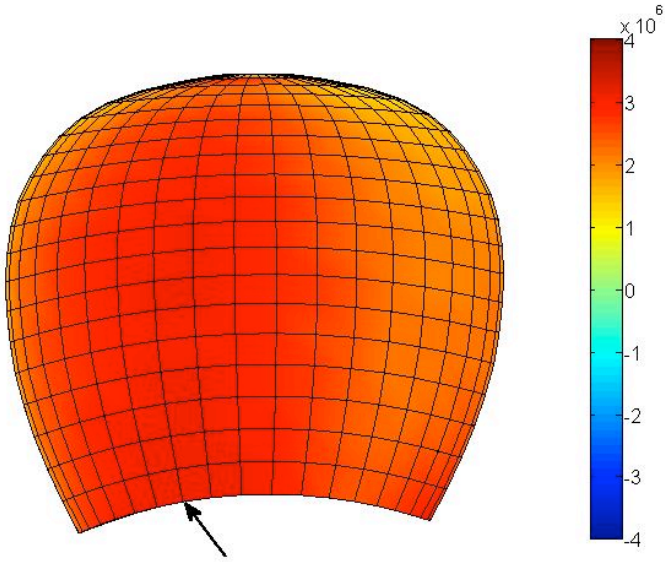

Figure 24: Point of Maximum Tensile Stress

In **Error! Reference source not found.**, plots of the maximum blade stress versus angular blade position for various ship speeds are shown. These plots also identify σ_a associated with each blade stress. Except for the highest ship speeds σ_a is relatively low, near the endurance limit for nickel, aluminum bronze, as shown in Figure 26.

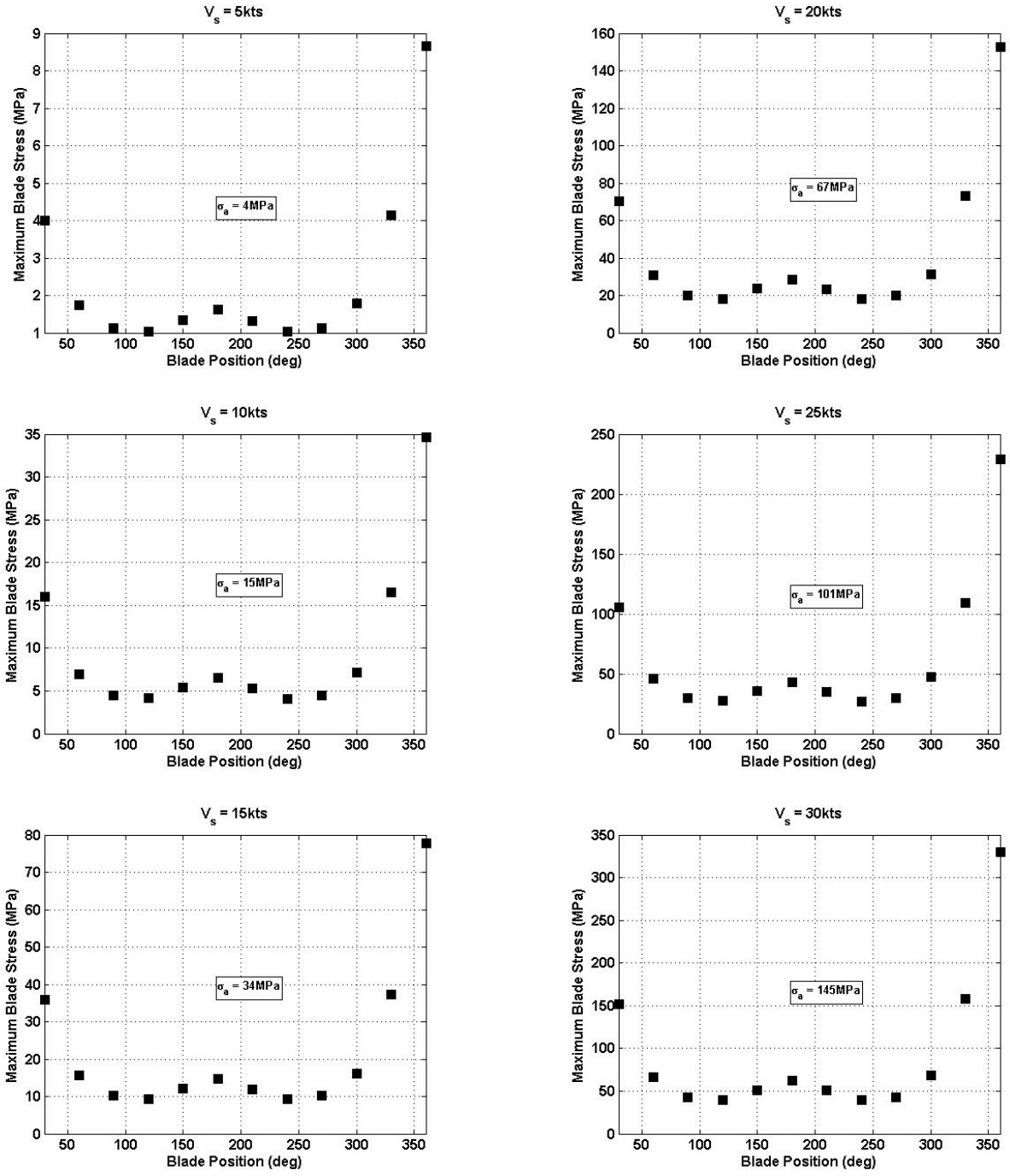

Figure 25: Maximum Blade Stress versus Angular Position for Various Ship Speeds

Fatigue Failure

Figure 26 shows a plot of alternating stress, σ_a, versus number of reversals/cycles to failure for nickel, aluminum bronze. Data for this figure was taken from Reference 10, detailed alloy composition and test condition are unknown. Ideally, one would design a propeller such that blade stresses were minimized in order to increase the fatigue life of the propeller.

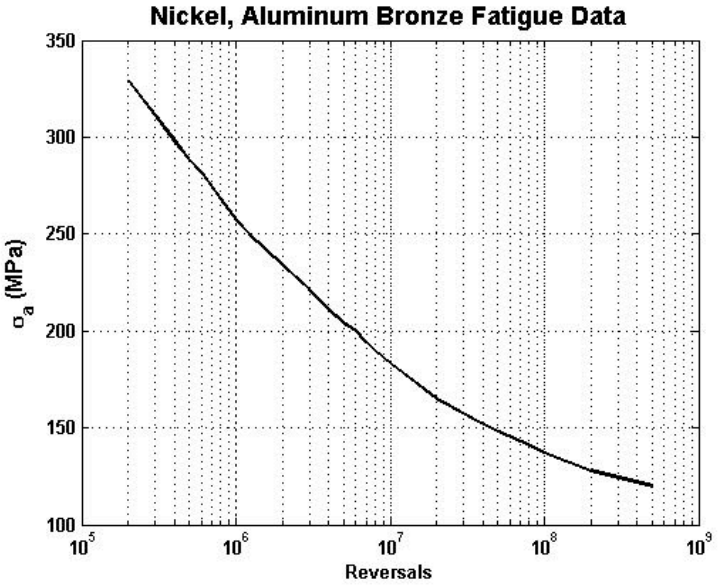

Figure 26: S-N Curve for NiAl Bronze

When performing a propeller fatigue analysis it is critical that the operational profile of the ship is taken into consideration. Figure 27 shows an operational profile for a warship which was taken from Reference 18. Since the propeller analyzed here was not analyzed for such a wide spectrum of speeds, Figure 28 was used in the example calculation.

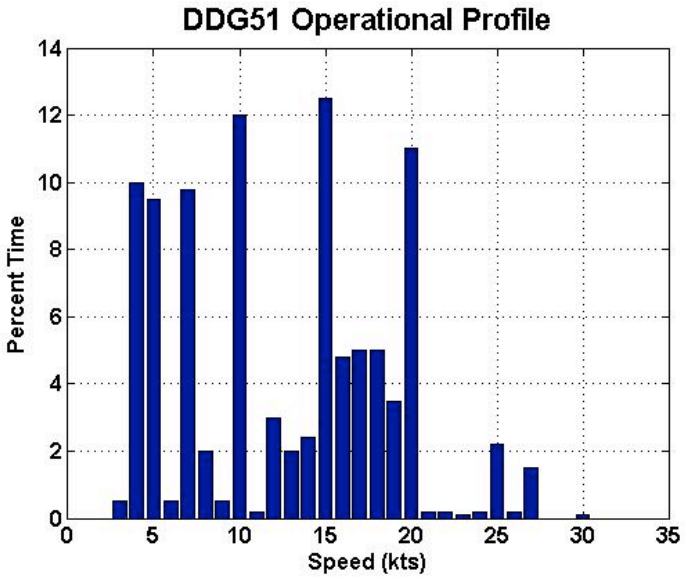

Figure 27: Operational Profile for DDG51

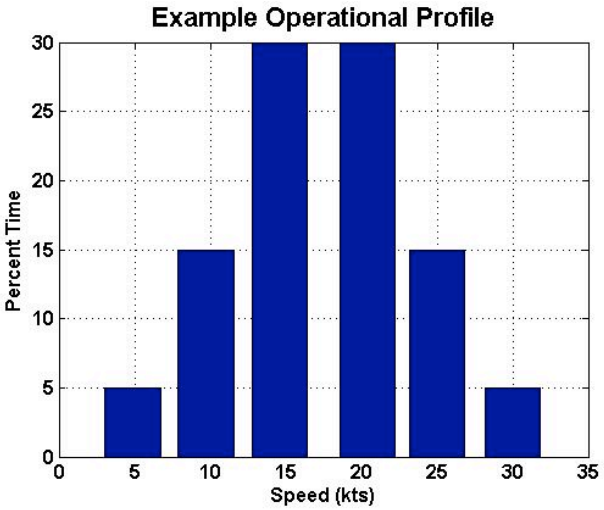

Figure 28: Example Operational Profile Used for Calculations

With the assumptions made in this analysis, there is a direct correlation between ship speed and blade stress. This correlation was used to produce Figure 29 below.

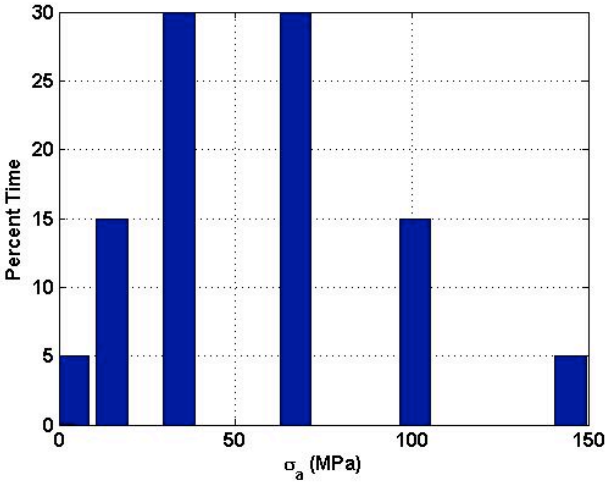

Figure 29: Time at Various Stress Levels

Miner's rule was used to predict the fatigue life of the propeller. Miner's rule is simply stated as shown in Equation 2.

$$\sum \frac{r_i}{R_i} = 1 \quad \textbf{16}$$

where
r_i = actual number of reversals at σ_a
R_i = reversals to failure at σ_a, determined from Figure 26.

In order to predict the fatigue life, additional equations are necessary. These are shown below.

$$r_i = RPM_i\, t_i \quad \textbf{17}$$

where
t_i = time spent at rotation rate, RPM_i
RPM_i = rotation rate which produces desired speed

$$t_i = x_i\, T \quad \textbf{18}$$

where
x_i = fraction of total time spent at RPM_i
T = total time of propeller operation

Substituting Equation 3 and Equation 4 into Equation 1 and solving for *T,* one obtains:

$$T = \frac{1}{\sum \frac{RPM_i\, x_i}{R_i}} \quad \textbf{19}$$

If one considers the blade stress at speeds below 25kts to be of infinite life then the fatigue life is 180 days. This calculation is dominated by the time spent at 30kts which is probably excessive when comparing Figure 28 and Figure 27.

Chapter 7 – Test Fixture Design and Construction

This chapter describes the design and construction of a test fixture for testing propellers and turbines. The test fixture described in this chapter was specifically designed for use in the hydrodynamics laboratory water tunnel at MIT but can also be used in a tow tank. The limitations of the test fixture are given in the Table 4.

Limits	Value	Basis
Torque	6 ft-lbf	Sensor limitation
Thrust	50 lbf	Sensor limitation
RPM	1500 rpm	Peak capability of motor
Current	18 amps	Peak capability of motor
Voltage	240 V-AC 300 V-DC	Required supply voltage Maximum controller output voltage

Table 4: Test Fixture Limitations

The design philosophy employed for this test fixture, with accompanying justification is given below.

1. Thrust and torque sensor must be the limiting component. The sensor used in this test fixture is on loan to Professor Richard Kimball from the US Navy. Searches for a commercially available sensor capable of simultaneous thrust and torque measurement did not yield any devices that could have been used in a test fixture of this size. Because of the limited availability of useable sensors, it was decided that the test fixture should be limited only by the sensor, to the maximum extent possible.
2. Components must be usable in other test fixtures. Since there were no other test fixtures of this type at MIT, this design constraint meant that the test fixture must be able to be disassembled and the components able to be used in other test fixture assemblies that might be designed by students in the future. This constraint was a significant driver in the selection of electrical components, manufacture of mechanical components and method of component assembly.
3. Fixture must be able to incorporate a high resolution encoder. This constraint effected the motor and encoder selection process.
4. Fixture must be capable of use in both a tow tank and water tunnel. This constraint drives the maximum allowable overall diameter, length and standpipe length of the test fixture.

Additional details concerning how the design philosophy impacted test fixture design as well as the final test fixture configuration are given in the sections that follow.

MECHANICAL

Thrust/Torque Sensor

The thrust/torque sensor used in this test fixture is a strain gage type sensor. The sensor uses two sets of strain gages; one set to measure thrust and the other set to measure torque. The strain gages are adhered to the center ring shown in Figure 30, which is covered in an opaque epoxy like material. The presence of this material introduced measurement error when building the CAD sensor model that was created and is one of the reasons why a factor of safety (FOS) of 2 was used when determining the maximum operational torque that could be applied to the sensor.

Since the sensor was to be the limiting component, it was necessary to characterize the thrust and torque capabilities of the sensor. In order to determine maximum thrust and torque the sensor could measure without damage, a determination of sensor material was made and finite element analysis (FEA) of the sensor was performed. For the purposes of this test fixture design, "damage" is defined as a load condition which would produce yielding in the sensor material. FEA required that a three dimensional model of the sensor be made, this model is shown in Figure 30.

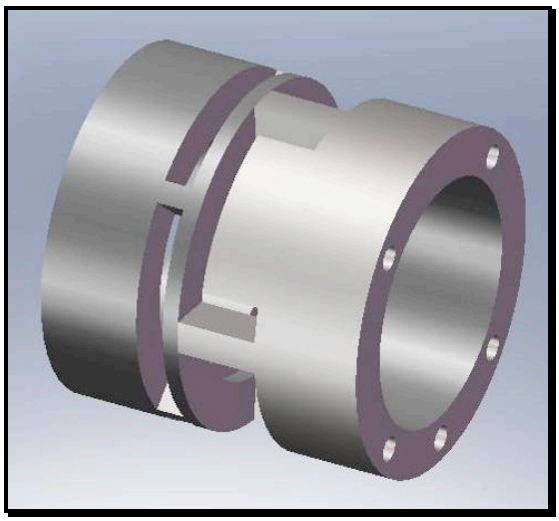

Figure 30: Provided Sensor

While measuring the sensor to determine physical dimensions for incorporation into the model, an inscription of 50lbf was found on one end of the sensor. 50lbf was used as the thrust load on the sensor in the FEA analysis in order to determine a FOS. The result of the FEA showed that the sensor can withstand a 50lbf axial load with an FOS of 2. The calculated stress distribution resulting from a 50lbf load is shown in Figure 31:

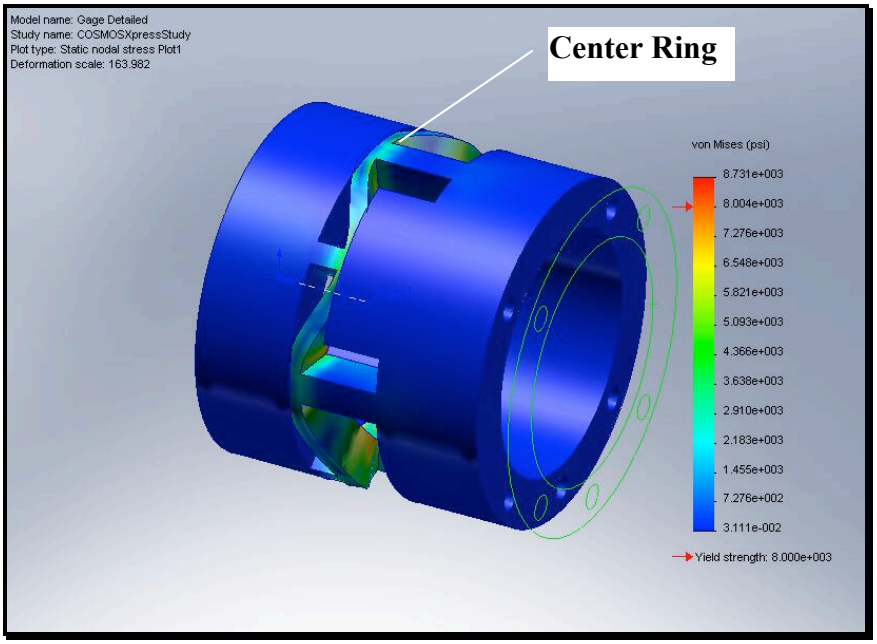

Figure 31: Stress from Axial Load on Sensor (50lbf applied)

The results of the FEA show interference between the center ring of the sensor and the end of the sensor. This interference is a result of the large scale factor necessary to make the sensor deflections visible and does not represent actual interference when the sensor is under a 50lbf thrust load.

In order to determine the maximum torque that the sensor could carry, a separate FEA was conducted. The results of this analysis show that the sensor could carry 12ft-lbf without damage. Application of a FOS of 2, that was determined from the thrust FEA, limited the maximum torque of the sensor to 6ft-lbf. A FOS of 2 is reasonable due to the dimensional error present in the model, described above, and a lack of validation of the FEA used on the model of the sensor. A picture of the stress distribution resulting from a 12ft-lbf applied torque is shown in Figure 32. Note that the "handle" that is present in the picture was necessary to be able apply a torque load in SolidWorks 2007 Education Edition.

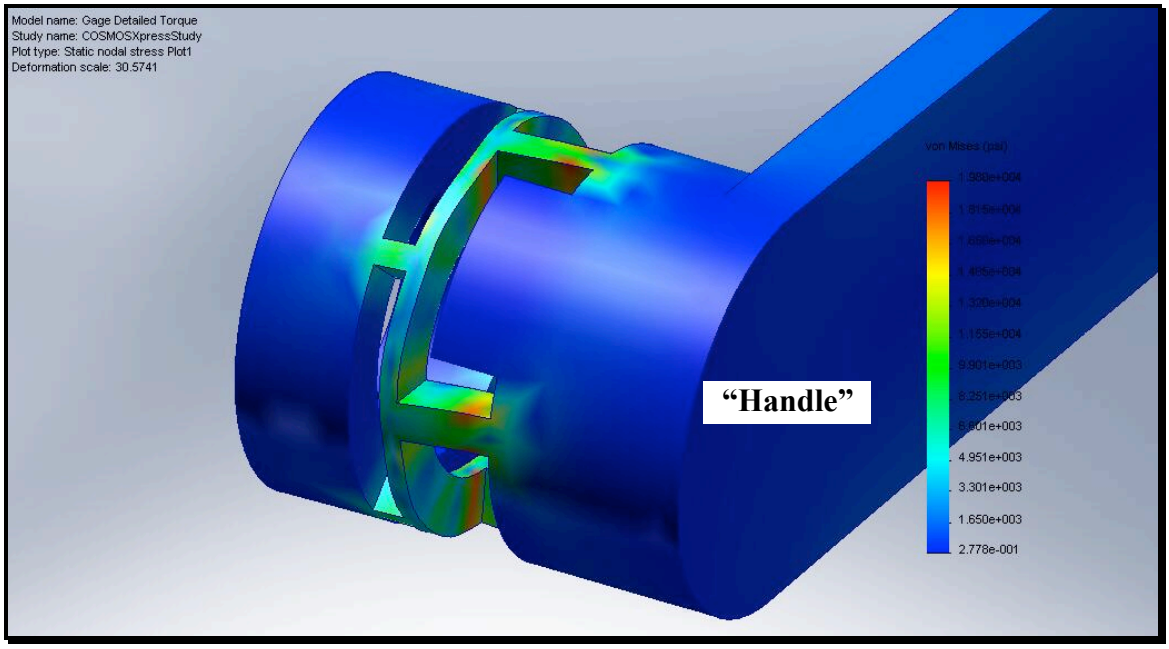

Figure 32: Stress from Torque Load on Sensor (12ft-lbf applied)

Output Shaft Configuration

Three options were considered for the configuration of the output shaft to which a propeller or turbine could be attached for testing.

1. A tapered shaft capable of accepting the fittings already manufactured and located in the water tunnel laboratory.
2. A straight shaft with a pin, similar to that used for propeller attachment to trolling motors.
3. A straight shaft with a flat side machined.

Option 1 was undesirable because the shaft size required to accommodate the taper would have required larger bearings and seals for the shaft which would have increased the friction resistance on the shaft and made sealing the shaft more difficult. Additionally, a larger diameter shaft has greater rotational inertia which would limit the rate at which the shaft could be accelerated during unsteady tests.

Option 3 was less desirable than Option 2 because of the complication of manufacturing propellers with a set screw hole. The intended manufacturing technique for propellers is 3D printing. Propellers manufactured using this method are made from ABS plastic. Successfully creating a threaded hole into this material with sufficient holding power for a set screw seemed unlikely. A second problem with this type of shaft is that it required a female section to be made in the propeller hub that would have been difficult to machine: a straight cylindrical hole that changes to a cylindrical hole with a flat. Previous experience manufacturing propellers using the 3D printing technique has shown that it is difficult to achieve a hub whose outer diameter is concentric to the drive shaft hole outer diameter. Therefore it is necessary to turn the propeller on a lathe to ensure that the drive shaft will easily attach to the propeller with minimal eccentricity between the inner and outer diameter of the propeller hub.

Option 2 requires that every propeller have a slot machined in the hub but this operation is simple using an end mill of the same size as the output shaft pin or printing the slot in the hub, if the turbine is manufactured using a rapid prototyping technique. Option 2 also requires that the end of the drive shaft be threaded to accept a nut to hold the propeller against the drive shaft pin, however these are external threads that are easy to manufacture. For these reasons, Option 2 for drive shaft configuration was chosen. A picture of the shaft is given Figure 33:

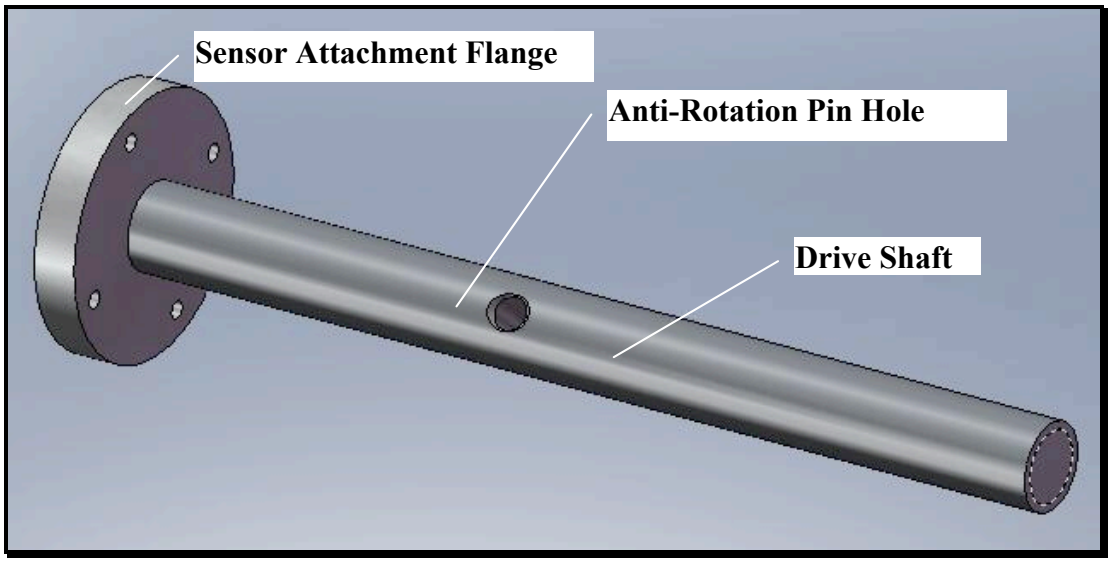

Figure 33: Output Shaft Configuration

Drive Shaft Configuration

The test fixture design described in this paper is intended to be used to test both propellers and turbines. Because of this dual use capability, it is necessary that the fixture be able to measure and support axial loads in two directions. Including the capability to support axial loads in two directions also protects the fixture from inadvertent damage should a load be applied in an axial direction for which the fixture was not designed.

Dual axial load support was accomplished by using two tapered roller bearings in an arrangement similar to the front wheel bearing assembly on an older automobile. The tapered roller bearings are mounted in a bearing assembly in such a way that one bearing supports the axial load in one direction and the second bearing supports the axial load in the other direction. The drive shaft in the vicinity of these bearings is threaded and slotted to accommodate an axle nut and star washer. The nut ensures the bearings are secured in the bearing housing and that the axial play in the drive shaft can be adjusted. The slot in the shaft, in combination with the star washer, ensures that the nut will not loosen. A picture of the drive shaft and bearing assembly is shown in Figure 34:

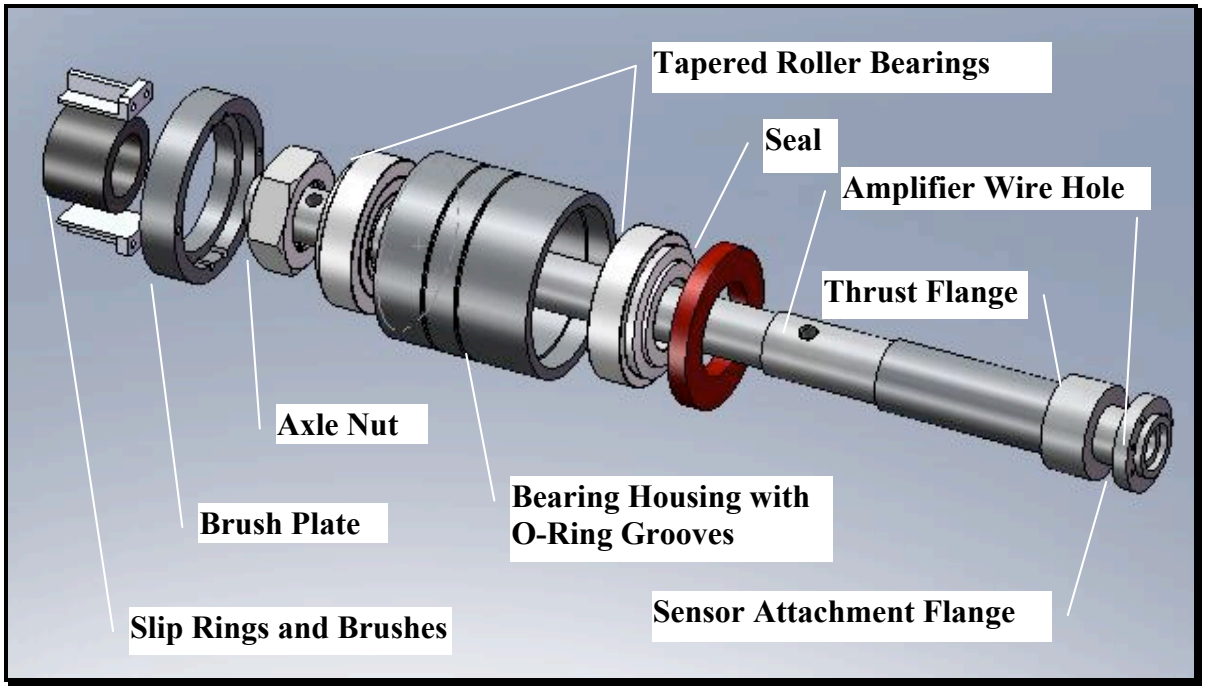

Figure 34: Driveshaft and Bearing Assembly with Brush Blocks and Slip Rings

The smallest diameter on the driveshaft was determined by the diameter of the slip ring assembly. Due to the shoulder required for the tapered roller bearings, the slip ring assembly can only be installed from one end of the shaft. The end of the shaft over which the slip rings must be moved to reach the installation location was made slightly smaller than the slip ring diameter in order to ease slip ring installation. The drive shaft diameter for installation of the slip rings is only slightly smaller than the shaft diameter required for the tapered roller bearings. This small change in diameter meant that little material was available to make the threads for the axle nut and therefore a custom nut, washer and thread configuration had to be manufactured.

Housings

Two assembly methods were considered for the external housings.

1. Threaded assembly
2. Shoulder fasteners

Using a threaded assembly has the advantage of minimizing the number of water leakage paths into the fixture and the number of o-rings required during assembly. The problem with a threaded assembly is that the threads can be difficult to manufacture, particularly for internal threads that run deep into the part, and large diameter threads are prone to seize in stainless steel. The problem with the shoulder fastener assembly method is that the number of leakage paths and o-rings required is significant and assembly requires that the components be precisely positioned prior to the installation of the shoulder fasteners. The shoulder fastener assembly method was chosen for ease of manufacture and the problem of water leakage paths was mitigated by installing the shoulder fasteners between a set of o-rings on the housing diameters.

ELECTRICAL

Slip Rings

As mentioned previously the torque/thrust sensor uses two sets of strain gages for load measurement. There are several possible methods to transmit the data signal from the sensor for recording. The method chosen for this fixture was to amplify the data signal at the sensor and then use a set of slip rings and brushes to conduct this signal to a point where a data acquisition system could be attached. This method was chosen for its simplicity.

The details of the slip ring assembly are included in the appendix. Six slip rings are required for sensor operation. Two are necessary to power both sets of strain gages, four rings are necessary for data signal transmission. The slip assembly used in this test fixture has eight slips rings in order to allow for future growth and to provide alternate slip rings should some become unusable. Each slip ring has four brushes riding on it, two from each brush block. The brushes from each brush block are soldered together so that four brushes are connected to each slip ring. Four brushes per slip ring are used in order to minimize the electrical resistance between the brushes and the slip rings. A photograph of the slip rings and brushes installed in the test fixture is shown in Figure 35:

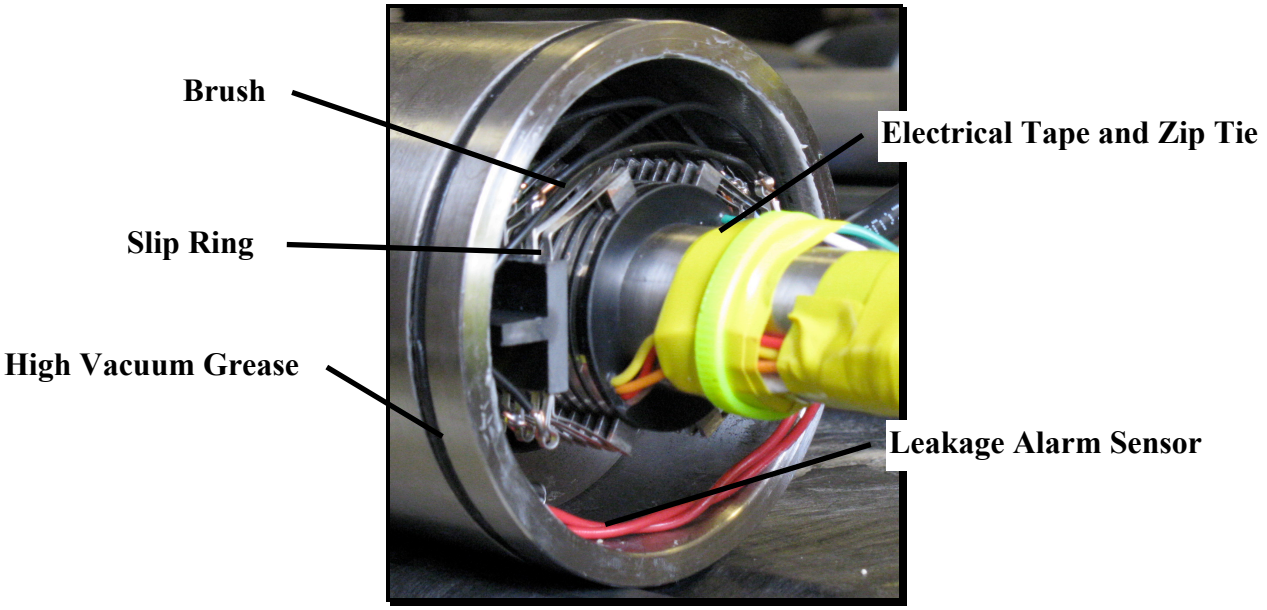

Figure 35: Installed Slip Rings and Brushes

In addition to the slip rings and brushes, Figure 35 shows two red wires near the bottom of the photograph. These wires are part of a leakage alarm system. If the ends of the two red wires are shorted, an audible alarm sounds indicating leakage into the test fixture. The yellow electrical tape and zip tie are present to secure the slip ring and strain gage amplifier wiring to the driveshaft. The connection of the slip ring wires and the stain gage amplifiers was made outside of the hollow drive shaft in order to ease assembly. The white substance on the end of the tube is a high vacuum silicone based grease that is applied to the surfaces prior to assembly in order ease assembly and as an additional measure to prevent leakage.

Amplifiers

Inside the thrust/torque sensor are two amplifiers. One amplifier is for the thrust data signal and the other is for the torque data signal. These amplifiers are mounted inside a piece of foam which is pressed into the sensor. The amplifiers that were purchased are designed for strain gage signal amplification for the motor sports industry and therefore represent a rugged option for signal amplification. Data signal amplification takes place as close to the sensor as possible in order to limit the data signal transmission loss and to prevent the signal to noise ratio of the data signal from becoming too low for practical use. Additional amplifier details are included in the appendix.

Motor

The desire to use the test fixture in the water tunnel limits the maximum allowable diameter of the test fixture. Previous experience with trolling motors in the water tunnel yielded good results. Trolling motor diameters ranged from 3.5 to 4 inches; therefore the maximum allowable test fixture diameter was set to 4 inches. A maximum diameter of 4 inches significantly restricts the available options for motor selection.

Another consideration in motor selection is the ability of the motor to also act as a generator in order to serve as a load for turbine testing. The requirement to also act as a generator further limits the choice of motor to those of a permanent magnet design. Although it is possible to use a motor without permanent magnets installed, the complication arising from supplying both the stator and rotor with electric current was deemed excessive for a test fixture.

The motor selected for this test fixture is a Parker kit motor, K089300. This motor is a DC brushless motor; the specific model selected also contains integral commutation. In selecting a motor, it was desirable to select a motor such that the sensor remained the limiting component in the design. Therefore a motor capable of torque in excess of 16N-m (12ft-lbf) was selected. A test fixture using a standard motor required a test fixture 6 inches in diameter.

A standard motor with the desired torque speed characteristics exceeded the maximum allowable diameter because a standard motor comes with a face plate on one end and electrical connectors on the other. The standard motor would have required customization to remove the electrical connectors and change the mounting configuration to a face frame mount. In addition to the complication and cost of performing the customization, supplying the motor with current would have also been challenging because the wires would have had to pass by/through the face plate area in order to be routed to the standpipe for passage out of the test fixture to the electrical supply

The K089 series motor has a maximum diameter of 3.5 inches which allows the motor to be attached inside a tube with a maximum outside diameter of 4 inches. The K089300 was selected because it is the highest torque motor listed in the catalogue for this series. Parker frameless kit motors generate additional torque in a given series by increasing the length of the stator windings and rotor. A kit motor has the following advantages:

1. Able to fit in a tighter package

2. Use of one shaft for both the motor and driveshaft which eliminates the need for a shaft coupling between motor shaft and propeller drive shaft
3. Stator windings are in direct contact with test fixture housing which make for efficient heat transfer out of the stator windings and into the fluid surrounding the test fixture.

The disadvantages of using a kit motor are:

1. Attachment of the motor into the fixture required that additional holes had to be drilled into the motor housing which meant an increase in the probability of a leak into the fixture.
2. Kit motors do not come with a high resolution angle encoder installed like the standard off the shelf motors.

The calculated torque speed curve for the K089300 is given in Figure 36. In both figures the dashed lines represent continuous operation while the solid lines represent peak or intermittent operation. The linear negative slope in the torque-speed curve is based on preventing the motor windings from overheating due to excess current.

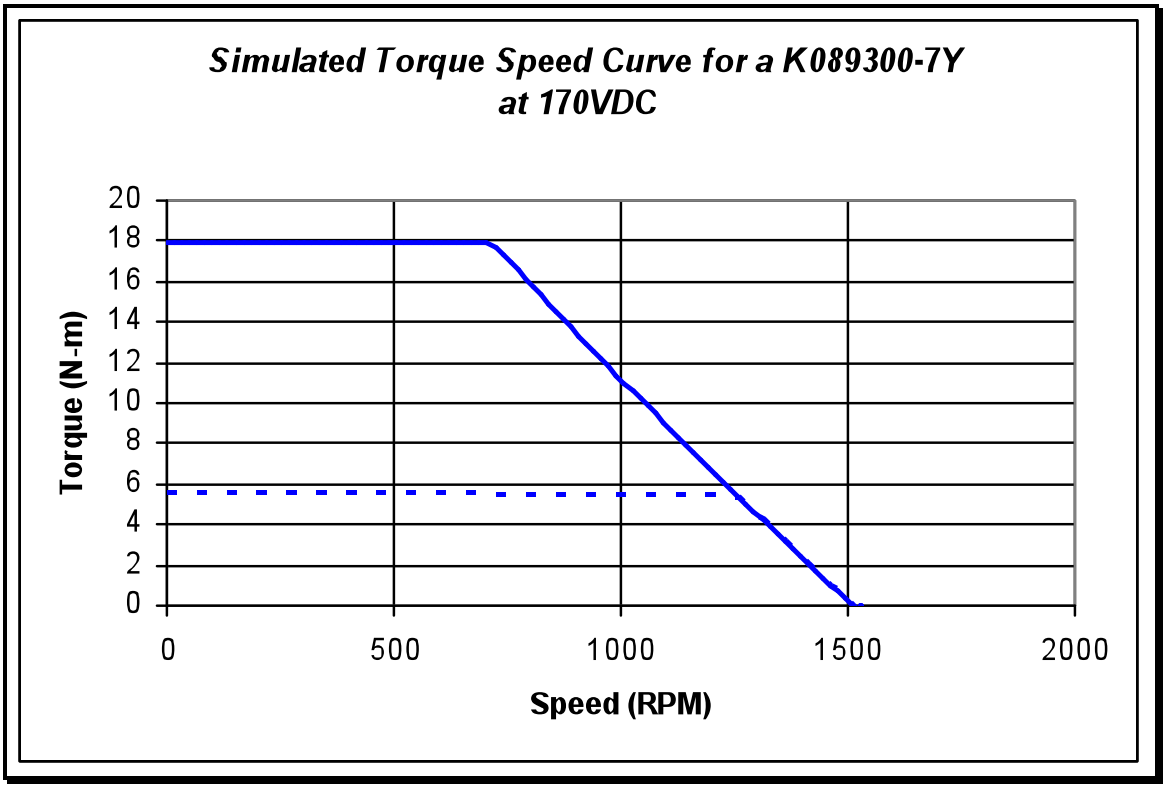

Figure 36: K089300-7Y Torque Speed Curve

The calculated power performance is given in Figure 37.

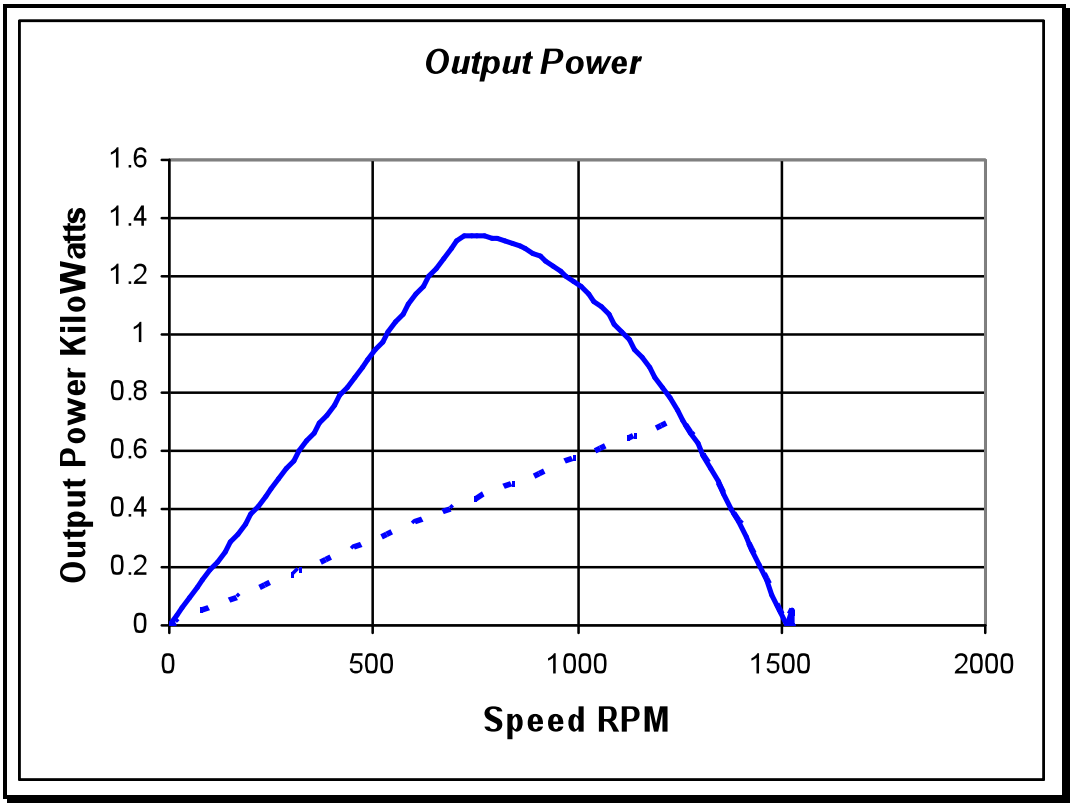

Figure 37: Output Power Capability

The current limitation of the motor is shown in Figure 38.

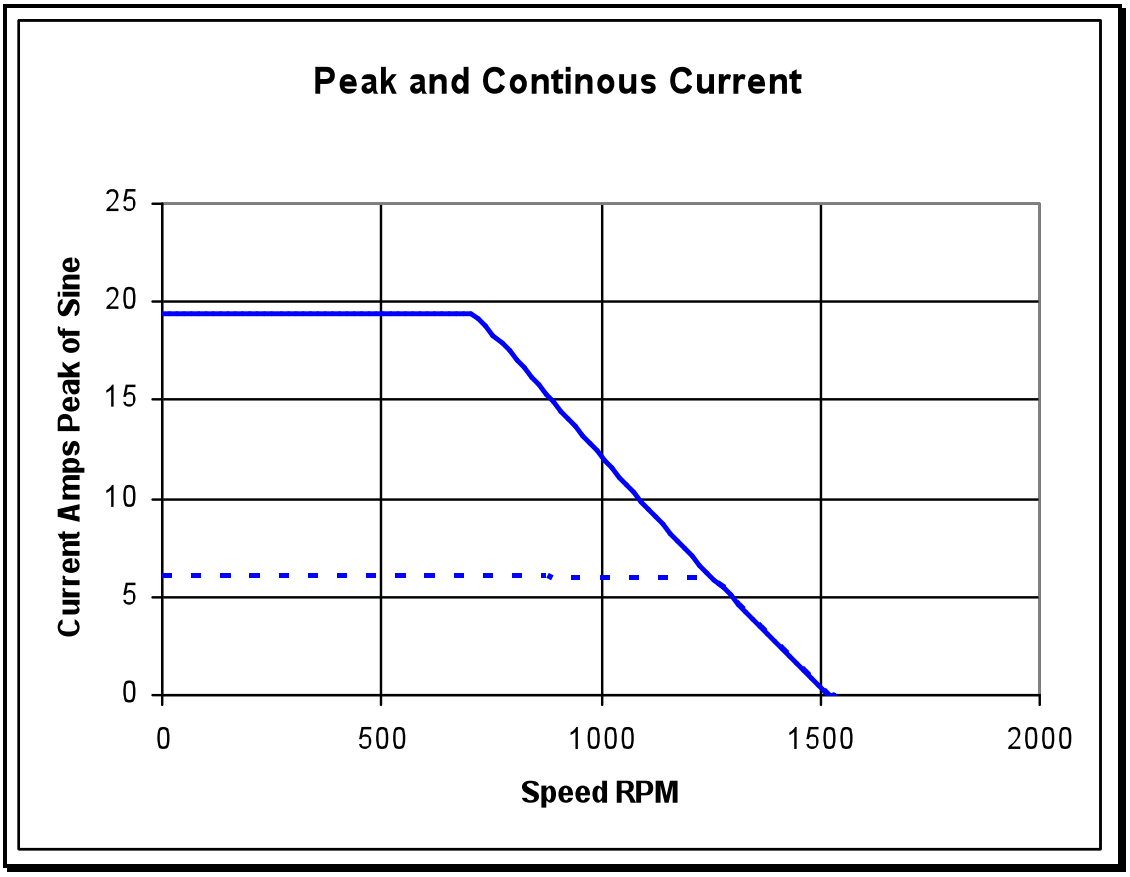

Figure 38: Limiting Current

Controller

In selecting a controller it was desirable to select a controller which could serve as both a motor controller and load controller, allowed for test fixture growth and had limited EMI emissions to prevent noise in the data signal. Students at the University of Maine have built and used a test fixture for cross flow turbines that used a Copley Xenus XTL-230-40 controller. They have been very pleased with the overall performance of their test fixture, particularly the low electrical noise generated by the controller. For these reasons the same controller and electrical layout were selected for this test fixture. Additional data on the controller is given in the controller data sheet in the appendix. A photograph of the electrical components in the enclosure is shown in Figure 39:

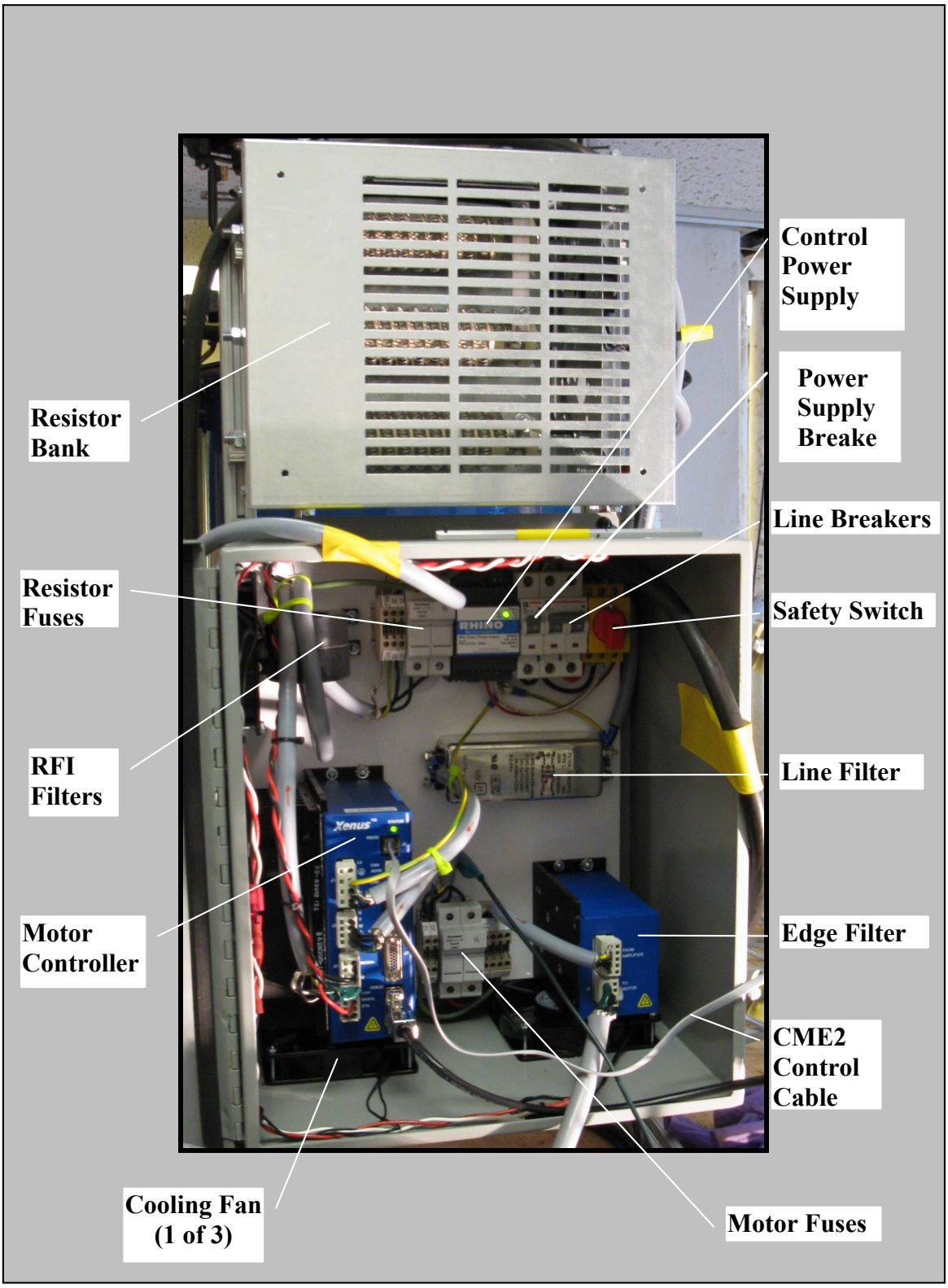

Figure 39: Electrical Components

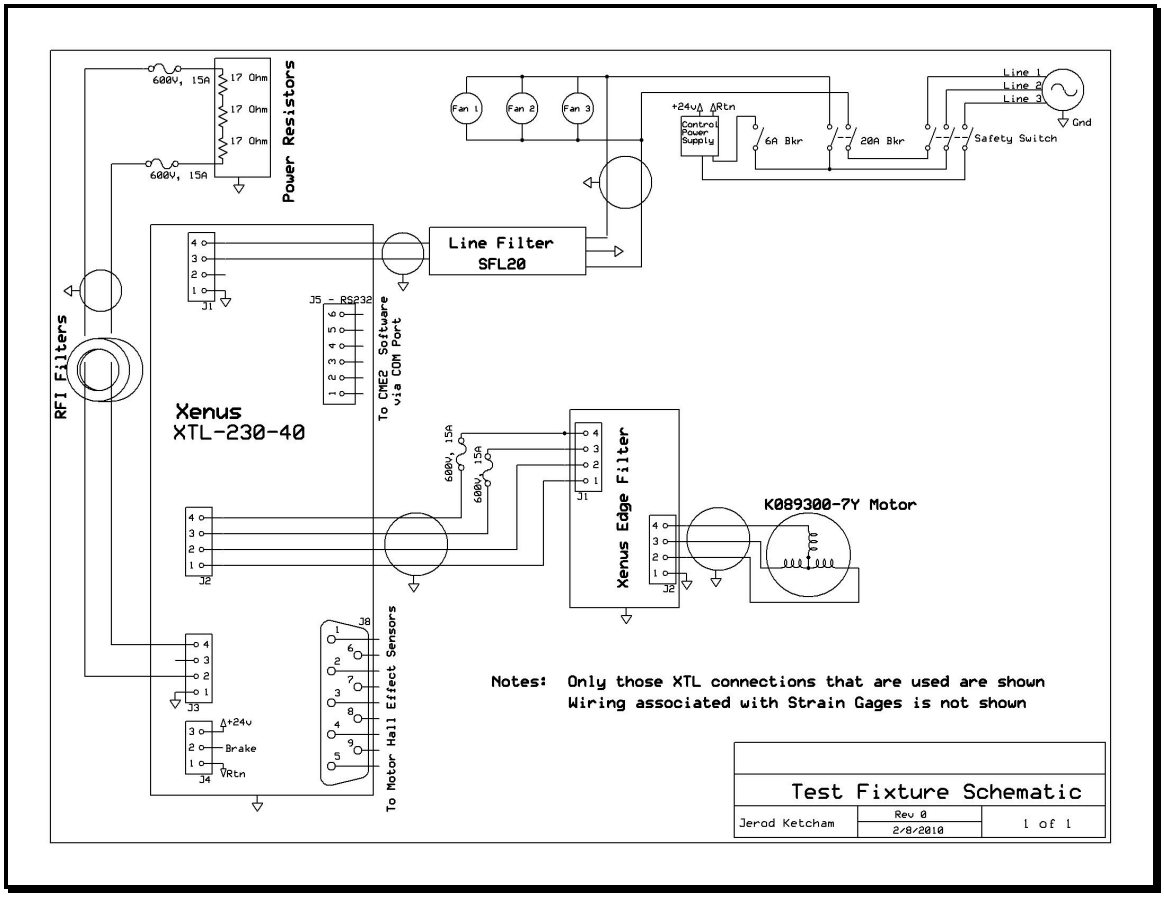

Figure 40: Schematic of Enclosure Electrical Components

A schematic of the components that are located inside the enclosure is shown in Figure 40. Note that all connections to the motor drive are not shown, only those connections that are used are shown. Strain gage wiring is a different circuit and is not shown in Figure 40.

CONSTRUCTION

The material used in the construction of the parts of the test fixture that could be in contact with the water is stainless steel. Depending on the part, the alloy is either a 303 or 304 stainless. These alloys were selected for their combination of corrosion resistance and machinability. Their corrosion resistance will be sufficient for use in a fresh water environment, however prolonged use in chlorinated water and use in saltwater should be avoided to prevent corrosion. All components in the test fixture are non-magnetic with the exception of the drive shaft and propeller shaft which became slightly magnetic as a result of the machining process. Two photographs of the completed test fixture in operation during turbine testing are shown in Figure 41.

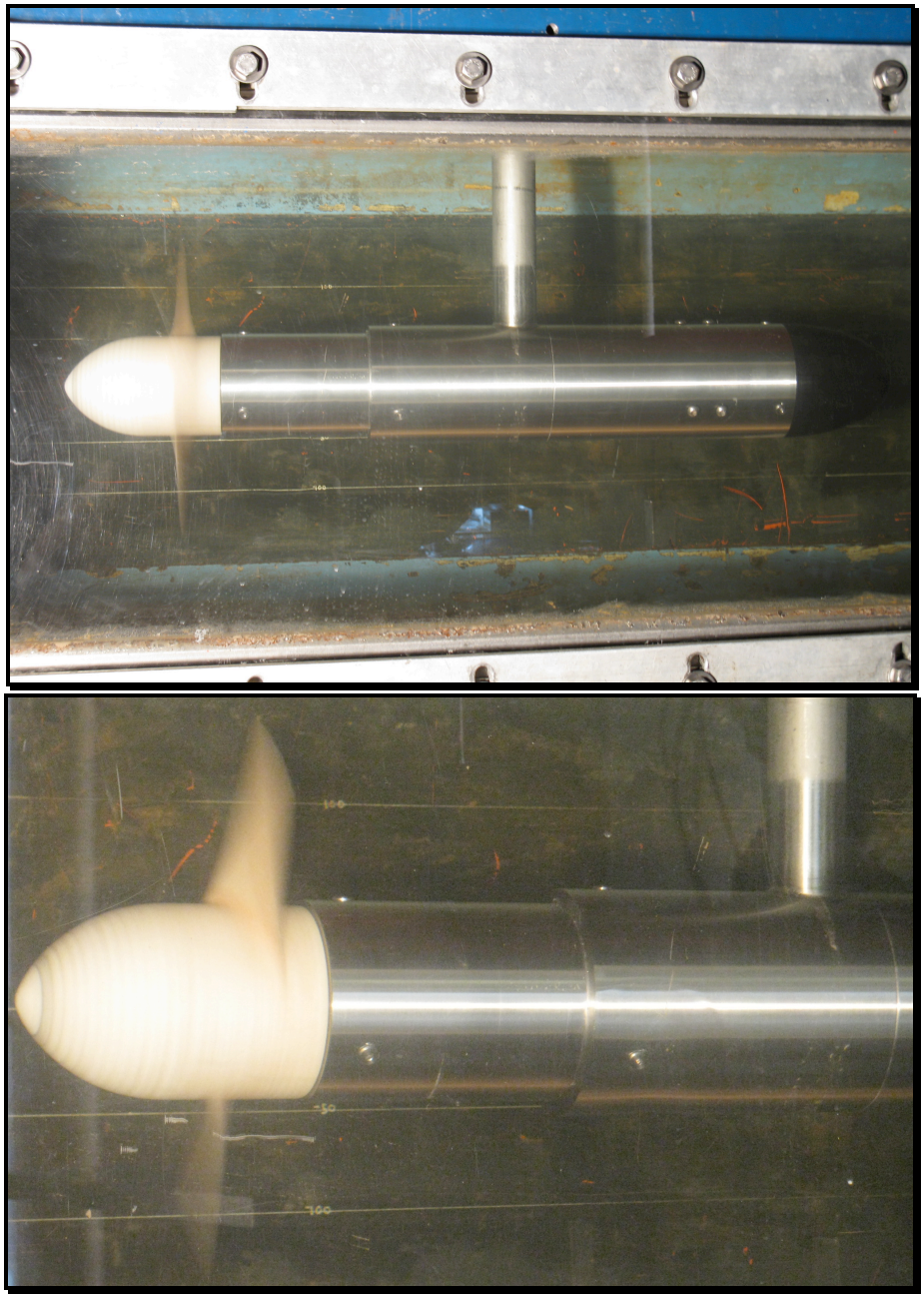

Figure 41: Completed Test Fixture in Operation

References

1. Benyon J.H. et al, *Engineering Against Fatigue*, A.A. Belkama, 1999
2. Carlton J.S., *Marine Propellers and Propulsion Second Edition*, Elsevier, 2007
3. Chung, H., *An Enhanced Propeller Design Program Based on Propeller Vortex Lattice Lifting Line Theory*, Master's Thesis MIT, 2007
4. Conway Joseph B., Sjodahl Lars H., *Analysis and Representation of Fatigue Data,* ASM International, 1991
5. D'Epagnier, K., *A Computational Tool for the Rapid Design and Prototyping of Propellers for Underwater Vehicles,* Master's Thesis MIT, 2007
6. Epps B., *An Impulse Framework for Hydrodynamic Force Analysis: Fish Propulsion, Water Entry of Spheres, and Marine Propellers*, PhD Thesis MIT, 2010
7. Epps, B. P. (SM); Stanway, M. J. (SM); and Kimball, R.W. (AM)., *OpenProp: An Open-source Design Tool for Propellers and Turbines,* SNAME Propellers and Shafting, 2009
8. Felli M., Felice F.D., *Propeller Wake Analysis in Nonuniform Inflow by LDV Sampling Techniques*, Journal of Marine Science and Technology, 2005
9. Harrington Roy L., *Marine Engineering*, Society of Naval Architects and Marine Engineers, 1992
10. Kerwin J.E. and Hadler J.B., *Principles of Naval Architecture, Propulsion*, SNAME, to appear 2010
11. Kerwin, J.E., *Hydrofoils and Propellers*. MIT course 2.23 notes, 2007.
12. Kimball, R.W.; Epps, B.P.; and M.J. Stanway, *OpenProp MATLAB code*. Open-source at http://openprop.mit.edu
13. Koronowicz, T., Chaja, P., Szantyr J., *A Computer System for the Complete Design of Ship Propellers*, Archives of Civil and Mechanical Engineering, 2008
14. Laskos, D., *Design and Cavitation Performance of Contra-Rotating Propellers*, Master's Thesis MIT, 2010
15. Peterson, C., *Minimum Pressure Envelope Cavitation Analysis Using Two-Dimensional Panel Method*, Master's Thesis MIT, 2008
16. Shigley Joseph E., Mischke Charles R., *Mechanical Engineering Design Fifth Edition*, McGraw-Hill Inc, 1989
17. Stubblefield, J.M., *Numerically-Based Ducted Propeller Design Using Vortex Lattice Lifting Line Theory*, Master's Thesis MIT, 2008
18. Gooding, T., *Principles in Naval Ship Design*, MIT course 2.703 notes, 2009
19. *Rules for Building and Classing Steel Vessels 2007*, American Bureau of Shipping, 2006

Appendix A – Codes

Moment of Inertia Calculation

function [Mp1, Ixc, Iyc, Ixyc, A, Xbar, Ybar, xl, yl, xu, yu] = MomentofInertia(xl,xu,yl,yu)

```
[Mp1,Np] = size(xu);

% Calculation of Section Area and Centroid
   for m=1:Mp1
      yshift = abs(min(yl(m,:)));     %Distance to shift all y points so that all are positive
      yu(m,:) = yu(m,:) + yshift;     %Shift of upper surface y points
      yl(m,:) = yl(m,:) + yshift;     %Shift of lower surface y points

      xshift = abs(min(min(xu(m,:)),min(xl(m,:))));   %Distance to shift all x points so that all are
                                                      positive
      xu(m,:) = xu(m,:) + xshift;                     %Shift of upper surface x points
      xl(m,:) = xl(m,:) + xshift;                     %Shift of lower surface x points

   end

   dxu = abs(diff(xu,1,2));
   dxl = abs(diff(xl,1,2));
   dyu = diff(yu,1,2);
   dyl = diff(yl,1,2);

   Ybar = zeros(1,Mp1);
   Xbar = Ybar;
   Ixc = Ybar;
   Iyc = Ybar;
   A = Ybar;
   Ixyc = Ybar;

   for m=1:Mp1
      hru = zeros(1,(Np-1));
      hrl = hru;
      htu = zeros(1,(Np-1));
      htl = htu;
      xctu = zeros(1,(Np-1));
      xctl = xctu;

      for n=1:(Np-1)
         hru(n)=min(yu(m,n),yu(m,n+1));   %Height of upper surface elemental rectangle
         htu(n)=max(yu(m,n),yu(m,n+1));   %Height of upper surface elemental trapezoid
         hrl(n)=min(yl(m,n),yl(m,n+1));   %Height of lower surface elemental rectangle
```

```
    htl(n)=max(yl(m,n),yl(m,n+1));      %Height of lower surface elemental trapezoid

    if dyu(m,n)<0
        xctu(n) = xu(m,n) + 2*dxu(m,n)/3;    %Distance from y-axis to upper surface
                                              elemental triangle centroid
    else
        xctu(n) = xu(m,n) + dxu(m,n)/3;      %Note: Value depends on whether left or right
                                              side of triangle is higher
    end

    if dyl(m,n)>0
        xctl(n) = xl(m,n) + 2*dxl(m,n)/3;    %Distance from y-axis to lower surface
                                              elemental triangle centroid
    else
        xctl(n) = xl(m,n) + dxl(m,n)/3;      %Note: Value depends on whether left or right
                                              side of triangle is higher
    end

end

xcru = xu(m,1:(Np-1))+dxu(m,:)/2;        %Distance from y-axis to upper surface
                                          elemental rectangle
xcrl = xl(m,1:(Np-1))+dxl(m,:)/2;        %Distance from y-axis to lower surface
                                          elemental rectangle

aru = dxu(m,:).*hru;              %Elemental upper surface rectangle area
atu = dxu(m,:).*(htu-hru)/2;      %Elemental upper surface triangle area
arl = dxl(m,:).*hrl;              %Elemental lower surface rectangle area
atl = dxl(m,:).*(htl-hrl)/2;      %Elemental lower surface triangle area

ycru = hru/2;                     %Distance from x-axis to upper surface elemental rectangle
                                  centroid
ycrl = hrl/2;                     %Distance from x-axis to lower surface elemental rectangle
                                  centroid
yctu = hru+(htu-hru)/3;           %Distance from x-axis to upper surface elemental triangle
                                  centroid
yctl = hrl+(htl-hrl)/3;           %Distance from x-axis to lower surface elemental triangle
                                  centroid


Mxsu = sum(ycru.*aru + yctu.*atu);    %1st moment of upper surface about x axis
Mxsl = sum(ycrl.*arl + yctl.*atl);    %1st moment of lower surface about x axis
Mxs = Mxsu - Mxsl;

Mysu = sum(xcru.*aru + xctu.*atu);     %1st moment of upper surface about y axis
Mysl = sum(xcrl.*arl + xctl.*atl);     %1st moment of lower surface about y axis
```

```
    Mys = Mysu - Mysl;

    Au = sum(aru + atu);          %Area of upper surface (x axis to upper surface)
    Al = sum(arl + atl);          %Area of lower surface (x axis to lower surface)
    A(m) = Au - Al;

    Ybar(m) = Mxs/A(m);       %Distance to centroid from x-axis
    Xbar(m) = Mys/A(m);       %Distance to centroid from y-axis

    %Uncomment lines below to see a section graph with centroidal axes
    %figure(m)
    %plot(xu(m,:),yu(m,:),xl(m,:),yl(m,:),'b')
    %line([min(xu(m,:)),max(xu(m,:))],[Ybar(m),Ybar(m)],'Color','r','LineWidth',2,'LineStyle','-
    -')
    %line([Xbar(m),Xbar(m)],[min(yl(m,:)),max(yu(m,:))],'Color','r','LineWidth',2,'LineStyle','-
    -')
    %axis equal
    %grid on
```

% Calculation of Section Moment of Inertia

```
    ixru = dxu(m,:).*hru.^3/3;
    ixyru = aru.*ycru.*xcru;
    ixtu = dxu(m,:).*(htu-hru).^3/36 + atu.*yctu.^2;
    ixytu = atu.*yctu.*xctu;

    ixrl = dxl(m,:).*hrl.^3/3;
    ixyrl = arl.*ycrl.*xcrl;
    ixtl = dxl(m,:).*(htl-hrl).^3/36 + atl.*yctl.^2;
    ixytl = atl.*yctl.*xctl;

    iyru = hru.*dxu(m,:).^3/12 + aru.*xcru.^2;
    iytu = (htu - hru).*dxu(m,:).^3/36 + atu.*xctu.^2;
    iyrl = hrl.*dxl(m,:).^3/12 + arl.*xcrl.^2;
    iytl = (htl - hrl).*dxl(m,:).^3/36 + atl.*xctl.^2;

    Ix = sum(ixru + ixtu) - sum(ixrl + ixtl);
    Iy = sum(iyru + iytu) - sum(iyrl + iytl);
    Ixy = sum(ixyru + ixytu) - sum(ixyrl + ixytl);

    Ixc(m) = Ix - A(m)*Ybar(m)^2;
    Iyc(m) = Iy - A(m)*Xbar(m)^2;
    Ixyc(m) = Ixy - A(m)*Xbar(m)*Ybar(m);
  end

end
```

Centrifugal Force Calculation

```
function [omega, Fc, Rdif] = CentrifugalForce(Mp1, N, R, A, RC, DR)

   %Initialization of Variables
   Fc = zeros(1,Mp1-1);
   Rdif = zeros(Mp1-1,Mp1-1);
   R1 = Rdif;

   omega = 2*pi*N/60;        %[rev/s] Rotation rate
   gamma = 1024.16;          %[kg/m^3] Density of ABS plastic
   % 8200;                   %[kg/m^3] Approximate density of Ni-Al-Bronze

   M = (omega)^2 * gamma * R^2;   %Multiplier used below

   %Calculation of centrifugal force on each section
   for m = 1:(Mp1-1)
     Fc(m) = M * sum(A(m:end-1).*RC(m:end).*DR(m:end)); %[N]
     R1(m,:) = RC - RC(m);
     I = find(R1(m,:)>0);
     Rdif(m,I) = R1(m,I);
   end

end
```

Stress Calculation

function [s] = Stress(CD, CL, BetaIC, Mp1, Np, xu, yu, xl, yl, rho, Vs, R, VSTAR, CoD, Rdif, DR, theta, Xbar, Ybar, Ixc, Iyc, Ixyc, Fc, A)

```
%Uncomment lines below to use Kerwin and Hadler method exactly
% eps = CD./CL;
% S = sin(BetaIC-eps);
% C = cos(BetaIC-eps);

S = sin(BetaIC);    %Factors for use below
C = cos(BetaIC);    %Factors for use below

%Initialization of Variables
INTQ = zeros(Mp1-1,Mp1-1);
INTT = INTQ;
MQ = zeros(1,Mp1-1);
MT = MQ;
Mxo = MQ;
Myo = MQ;
s = zeros(Mp1-1,2*Np);

%Concatenation of upper and lower section curves into a single curve
Xu = xu(:,:);
Yu = yu(:,:);
xs = cat(2,Xu,fliplr(xl));
ys = cat(2,Yu,fliplr(yl));

%Uncomment lines below to see a plot of root blade section
% axes('fontweight','bold')
% hold on
% plot(xs(1,:),ys(1,:),'-ks','LineWidth',2)
% axis equal
% title('Root Section Plot','Fontweight','bold', 'Fontsize', 14)
% xlabel('X (m)','Fontweight','bold','Fontsize',12)
% ylabel('Y (m)','Fontweight','bold','Fontsize',12)

M = rho*Vs^2*R^3;                %Multiplier used below
for m=1:(Mp1-1)
   %Uncomment two lines below to use Kerwin and Hadler method exactly
   %INTQ(m,:) = M* (VSTAR.^2 .* CL .* CoD .* Rdif(m,:) .*S .*DR);
   %INTT(m,:) = M* (VSTAR.^2 .* CL .* CoD .* Rdif(m,:) .*C .*DR);
   INTQ(m,:) = M* (VSTAR.^2 .* (CL .*S + CD.*C).* CoD .* Rdif(m,:).*DR);
   INTT(m,:) = M* (VSTAR.^2 .* (CL .*C - CD.*S).* CoD .* Rdif(m,:).*DR);
```

```
    MQ(m) = sum(INTQ(m,:));
    MT(m) = sum(INTT(m,:));
    Mxo(m) = MT(m)*cos(theta(m)) + MQ(m)*sin(theta(m));
    Myo(m) = MT(m)*sin(theta(m)) - MQ(m)*cos(theta(m));

    xsdiff(m,:) = xs(m,:) - Xbar(m);

    ysdiff(m,:) = ys(m,:) - Ybar(m);

    s(m,:) = ((-Mxo(m)*Iyc(m) + Myo(m)*Ixyc(m))*ysdiff(m,:) - (-Mxo(m)*Ixyc(m) +
    Myo(m)*Ixc(m))*xsdiff(m,:)) / (Ixc(m)*Iyc(m) - Ixyc(m)^2) + Fc(m)/A(m);

    %Uncomment line below to use a more exact equation for stress which
    %takes into account the product of inertia
    %s(m,:) = ((-Mxo(m)*Iyc(m) + Myo(m)*Ixyc(m))*ys(m,:) - (-Mxo(m)*Ixyc(m) +
    Myo(m)*Ixc(m))*xs(m,:)) / (Ixc(m)*Iyc(m) - Ixyc(m)^2) + Fc(m)/A(m);

    %Uncomment lines below for plots of stress on each blade section
    % figure(m)
    % %     plot3(xs(m,:),ys(m,:),s(m,:),'rs')
    % %     grid on
    % %     xlim([min(xs(m,:)),max(xs(m,:))])
    % %     ylim(xlim)
    % patch(xs(m,:),ys(m,:),s(m,:))
    % colormap(jet)
    % colorbar
    % grid on
    % axis equal
  end
  clear CL

end
```

Blade Stress Plots

```
function [] = Plot_Blade_Contours(X3D,Y3D,Z3D,s,plottitle)

   [rows,cols]=size(X3D);  %X3D is from the geometry.m module
   Mp = rows-1;            %Number of blade sections

%Concatenate matrices to create vertex matrix for patch function.  This is necessary because
the patch function expects a matrix whose rows are the vertices in x,y,z coordinates.
   colx = X3D(1,:)';
   coly = Y3D(1,:)';
   colz = Z3D(1,:)';
   colS = s(1,:)';
   for n=2:rows-1
      colx = vertcat(colx,X3D(n,:)');
      coly = vertcat(coly,Y3D(n,:)');
      colz = vertcat(colz,Z3D(n,:)');
      colS = vertcat(colS,s(n,:)');
   end

%Create face matrix for patch function- this tells the patch function how to connect the
vertices to create a face.  This code uses a square/rectangular face.
   F(:,1) = 1:cols*(Mp-1);
   F(:,2) = F(:,1) + 1;
   F(:,3) = F(:,1) + (cols+1);
   F(:,4) = F(:,1) + cols;

%Create special rows - the pattern of face vertices "wraps," these lines make the pattern wrap
properly
   m = 0:cols:cols*(Mp-1);
   for n = 1:length(m)
      if m(n)>1
         F(m(n),1:4) = [F(m(n),1), F(m(n),1)-(cols-1), F(m(n),1)+1, F(m(n),1)+4];
      end
   end

%Remove extra face matrix rows - This removes "extra" rows from wrapping scheme above
   Fa = F(1:cols-1,:);
   for o=1:Mp-2
   Fa = vertcat(Fa, F(o*cols+1:(o+1)*cols-1,:));
   end


    % Create Vertices matrix
    a = [colx,coly,colz];
```

```
    % Create Figure
    figure1 = figure('Color',[1 1 1]);

    % Create axes
    axes('Visible','off','Parent',figure1,'CLim',[-4e+006 4e+006]);
    view([-83 2]);
    colorbar('FontWeight','bold')
    title(plottitle,'Visible','On','FontSize',14,'FontWeight','bold')

    % Call patch function
    patch('Vertices',a,'Faces',Fa,'FaceVertexCData',colS,'FaceColor','interp','FaceLighting','goura
    ud')

    % Uncomment line below and adjust numbers to set colorbar scale
    % axis('CLim',[-2e+008 2e+008])

end
```

Usage Script

Load Variables

```
D = pt.geometry.D;              %Propeller Diameter
N = pt.geometry.N;              %Propeller rotation rate [RPM]
RC = pt.design.RC;              %Control Point (Section) Radius []
DR = pt.design.DR;              %Control Point Radius Difference []
VSTAR = pt.design.VSTAR;        %Total inflow velocity []
TANBC = pt.design.TANBC;        %Tangent of inflow angle for each Control Point
BetaIC = pt.design.BetaIC;      %Ideal inflow angle for each Control Point
CL = pt.design.CL;              %On design Lift Coefficient for each Control Point
CD = pt.design.CD;        %On design Drag Coefficient for each Control Point
CoD = pt.design.CoD;      %Chord Length/Diameter for each Control Point
xu = pt.geometry.xu;      %Upper section x points - Leading edge to trailing edge
yu = pt.geometry.yu;      %Upper section y points - Leading edge to trailing edge
xl = pt.geometry.xl;      %Lower section x points - Leading edge to trailing edge
yl = pt.geometry.yl;      %Lower section y points - Leading edge to trailing edge
X3D = pt.geometry.X3D; %x points which create blade surface
Y3D = pt.geometry.Y3D; %y points which create blade surface
Z3D = pt.geometry.Z3D;  %z points which create blade surface
UASTAR = pt.design.UASTAR; %Axial blade influence velocity []
UTSTAR = pt.design.UTSTAR;  %Tangential blade influence velocity []
Vs = pt.input.Vs;         %Design ship speed [m/s]
Js = pt.input.Js;         %Design Advance Coefficient
alpha = pt.design.alpha;  %[deg] Section angle of attack

theta = pi/180 * pt.geometry.theta; %Pitch angle in radians
```

Section Centroid and Moments of Inertia Calculation

```
[Mp1, Ixc, Iyc, Ixyc, A, Xbar, Ybar, xl, yl, xu, yu] = MomentofInertia(xl,xu,yl,yu);
```

Centrifugal Force

```
[omega, Fc, Rdif] = CentrifugalForce(Mp1, N, R, A, RC, DR);
```

Stress Calculation

```
[s] = Stress(CD, CL, BetaIC, Mp1, Np, xu, yu, xl, yl, rho, Vs, R, VSTAR, CoD, Rdif, DR,
theta, Xbar, Ybar, Ixc, Iyc, Ixyc, Fc, A);
```

Make Stress Plot

```
Plot_Blade_Contours(X3D, Y3D, Z3D, s, 'Suction Side')
```

Appendix B – Parts List

Appendix C – Drawings